MEASUREMENT OF $\psi(2S)$ DECAYS INTO $\Lambda\overline{\Lambda}\pi^+\pi^-$

MUHAMMAD MUSHRAF ANSARI

Centre for High Energy Physics
University of the Punjab
Lahore-54590, Pakistan

(August, 2012)

MEASUREMENT OF $\psi(2S)$ DECAYS INTO $\Lambda\overline{\Lambda}\pi^+\pi^-$

by

MUHAMMAD MUSHRAF ANSARI

Submitted in Partial Fulfillment of the Requirements for the Degree of DOCTOR OF PHILOSOPHY

at

Centre for High Energy Physics
University of the Punjab
Lahore-54590, Pakistan

(August, 2012)

To My Parents

&

Wife

CERTIFICATE

It is certified that I have read this dissertation and that, in my opinion, it is fully adequate in scope and quality for the degree of Doctor of Philosophy.

(Prof. Shan Jin)
Supervisor

(Prof.Dr. Haris Rashid)
Supervisor

Submitted through

(Prof. Dr. Haris Rashid)
Supervisor & Director

DECLARATION

This work represents the effort of the members of BES III group at the Centre for High Energy Physics, University of the Punjab Lahore, Pakistan. I claim the credit for the analysis and final results presented in this thesis which are entirely my own and were compiled as a member of BES III group at CHEP.

This thesis which is being submitted for the award of degree of Ph.D in the University of the Punjab does not contain any material which has been submitted for the award of any other degree or diploma in any university. To the best of my knowledge and belief, it does not contain any material published or written by another person except due references are made to the source in the text of the thesis. If any reference is found missing that would be completely unintentional and I do not have any pretension to own the credit for that.

Muhammad Mushraf Ansari

Acknowledgments

All praise for "ALMIGHTY ALLAH", whose Uniqueness, Oneness, and Wholeness is unchangeable, who guided me in difficult and congeal circumstances during my research work. All respects for the Holy Prophet "Hazrat MUHAMMAD (PBUH)", who provided us the unique and complete path of life.

I am grateful to my supervisors; Prof. Dr. Haris Rashid and Prof. Shan Jin, for their time and effort in discussion of analysis and preparation of this thesis and their support over the years. Their patience, insight and advice have provided me guidance through the process of selecting, designing and performing the analysis. It was a great pleasure to work under their supervision.

I am extremely thankful to the BESIII Collaboration, especially officials of Institute of High Energy Physics, Beijing, China, for allowing to use BESIII data and computing resources for my research work.

I am also thankful to BESIII group at Centre for High Energy Physics, University of the Punjab, for providing me day and night facilities for using online BESIII computing resources to accomplish physics analysis of BESIII experimental data.

An important contribution to the success of this work is the continuing financial support from the Higher Education Commission, Pakistan, which allowed me to direct all my efforts towards the research work.

I express my sincere thanks to Dr. Talab Hussain for his cooperation in performing this analysis. From him I learnt a lot about analysis techniques and strategies. He provided me a lot of guidance and advice at the beginning of this work. He also provided great technical helps during the period of this analysis.

I would like to acknowledge Dr. Abrar Ahmad Zafar who helped me to get expertise in data analysis tools and software and to discuss the analysis results during my work at Centre for High Energy Physics.

I would like to thank my friends and colleagues; Mr. S. M. Sohail Gilani, Mr. Azmat Iqbal and Mr. Anjum Javed, for their encouragement throughout my research work.

I wish to express my deepest gratitude to my loving parents, my sisters and my brothers, for their enduring and whole-hearted support.

I am very grateful to my wife for her encouragement during all the years I was preoccupied with this research work.

Muhammad Mushraf Ansari

List of Figures

List of Tables

Abstract

This analysis is based on 106 M $\psi(2S)$ data collected with Beijing Spectrometer III (BESIII) detector at Beijing Electron Positron Collider II. We report improved measurements of the branching fractions of $\psi(2S) \to \Lambda\overline{\Lambda}\pi^+\pi^-$, $\psi(2S) \to \Xi^-\overline{\Xi}^+$ and $\psi(2S) \to \Sigma^{*+}\overline{\Sigma}^{*-}$. The branching fractions measured are $(1.34 \pm 0.05_{stat} \pm 0.24_{sys}) \times 10^{-4}$, $(3.15 \pm 0.35_{stat} \pm 0.55_{sys}) \times 10^{-5}$ and $(3.39 \pm 0.34_{stat} \pm 0.61_{sys}) \times 10^{-5}$, respectively.

Contents

Chapter 1

Introduction

Particle Physics deals with unraveling the fundamental nature of the universe. This task may be performed in two ways; either theoretically or experimentally [1]. On theoretical side, Standard Model of Particle Physics provides the best mathematical formalism to investigate the fundamental issues of the universe [2, 3]. Experimentally, scientists have been trying to uncover the fundamental mysteries of the universe for several decades. Currently, there are numerous high energy physics experiments which are producing huge amounts of data needed for approaching feasible answers about the fundamental nature of the universe [4]. In this direction, an extremely important discovery was made by two high energy physics groups at SLAC (Stanford Linear Accelerator Center) and BNL (BrookHaven National Laboratory) in 1974 [5, 6]. They simultaneously discovered a new resonance composed of a pair of charm quark and its anti-quark, called charmonium with quantum numbers: $J^{PC} = 1^{--}$. This state was given the name; J/ψ. After ten days, its first excited state $\psi(2S)$ was also discovered [7]. After that, a chain of

discoveries started.

Due to the heavy mass of charm quark, the charmonium system can be treated as a non-relativistic bound state [8]. Since the discovery of J/ψ, many efforts have been made to understand the charmonium spectrum and its properties. The charmonium properties can be investigated through detailed analysis of different decay modes of charmonia. On this side, most of the experiments were performed at electron positron colliders. The main advantage of these experiments is the direct access of the states with $J^{PC} = 1^{--}$. Currently, an experiment is being performed at Beijing Electron-Positron Collider II (BEPCII) using Beijing Spectrometer III (BESIII). This experiment is providing huge amounts of charmonium data (at J/ψ and $\psi(2S)$ central mass values, etc.) which can be used for studying key properties of charmonia. In this work, we have used 106 million $\psi(2S)$ data accumulated by BES III detector, to measure the branching fractions of $\psi(2S)$ decays into $\Lambda\bar{\Lambda}\pi^+\pi^-$. This work provides more precise measurements of the branching ratios of $\psi(2S) \to \Lambda\bar{\Lambda}\pi^+\pi^-$, $\psi(2S) \to \Xi^-\bar{\Xi}^+$ and $\psi(2S) \to \Sigma^{*+}\bar{\Sigma}^{*-}$ to be $(1.34 \pm 0.05_{stat} \pm 0.24_{sys}) \times 10^{-4}$, $(3.15 \pm 0.35_{stat} \pm 0.55_{sys}) \times 10^{-5}$ and $(3.39 \pm 0.34_{stat} \pm 0.61_{sys}) \times 10^{-5}$, respectively. The previously measured values are $(2.8 \pm 0.5) \times 10^{-4}$, $(18 \pm 6) \times 10^{-5}$ and $(11 \pm 4) \times 10^{-5}$, respectively.

Before going onto the details of the analysis work, in the following chapter, we will highlight the important concepts of particle physics: Standard Model of Particle Physics, charmonium spectroscopy and BESIII experimental setup.

Chapter 2

Fundamental Concepts

It is known from the human history that the composition of universe has always been a subject of great interest. It happened right from the discovery of the atom that the theoretical studies and experimental observations have allowed us to understand the fundamental nature of the universe in more depth. It is now believed that all the matter we see around is made of leptons, quarks and the gauge bosons [9]. The leptons and quarks are the constituents of the composite particles and the gauge bosons are the mediating particles of the fundamental forces [10]. The most successful model that provides the understanding of the fundamental nature of matter is *the Standard Model*. It has been developed as a framework for understanding the properties of fundamental or elementary particles and their interactions[11]. The standard model has been incredibly consistent with the experimental observations.

2.1 Particle Phenomenology

2.1.1 Leptons

Leptons are fundamental particles in the standard model. They are spin half particles (fermions) and cannot participate in strong interaction [12]. There are six leptons: electron (e^-), muon (μ^-), tauon (τ^-), electron neutrino (ν_e), muon neutrino (ν_μ) and tauon neutrino (ν_τ). First three particles are charged while the rest are neutral. They are grouped in three generation. Corresponding to leptons that carry negative charge, there exist anti-leptons with opposite charge [13].

2.1.2 Quarks

The idea of quark was first introduced by Murray Gell-Mann and George Zweig in 1964 [14]. They postulated that all the matter is composed of spin 1/2 particles, termed as quarks. There are six kind of quarks which are characterized by their flavour and paired in three generations. The *up (u)* and *down (d)* quarks, the most stable and lightest particles, belong to first generation of quarks . Most of the matter in the universe is made up from the particles belonging to first generation. The *charm (c)* and *strange (s)* quarks belong to second while *top (t)* and *bottom (b)* ones belong to third generation. Quarks in second and third generations are heavier and decay to the most stable generation [15]. The quarks have fractional charge Q = $+2/3e$ and Q = $-1/3e$, where e is the fundamental electric charge. Greenberg postulated that quarks have another quantum number, *colour* also known as colour

charge, which keeps the quarks in the bound state [16]. Quarks interact via strong, electromagnetic and weak interactions. The properties of quarks are shown in the Table 2.1.

Table 2.1: *Properties of quarks*

Generation	Quark Name	Symbol	Mass (GeV/c^2)	charge
First Generation				
	Down	d	≈ 0.3	-1/3e
	Up	u	≈ 0.3	2/3e
Second Generation				
	Strange	s	≈ 0.5	-1/3e
	Charm	c	≈ 1.5	2/3e
Third Generation				
	Bottom	b	≈ 4.5	-1/3e
	Top	t	≈ 174	2/3e

In addition to quarks there are corresponding anti-quarks having same mass but opposite charge.

2.1.3 Hadrons

Although no isolated quarks have been observed experimentally, instead their evidences are found in the form of their bound states called hadrons. Only three bound states of quarks exist, baryons, anti-baryons and the mesons. According to constituent quark model, baryons and anti-baryons are the bound states of three quarks and three anti-quarks respectively with half-integral spin. Meson is the bound state of a quark and anti-quark [17]. Although quarks carry fractional charge, they combine in such a way that hadrons have net integral charge and no colour charge. Our study involves four mesons and two baryons in the final state and we discuss them briefly.

2.1.4 Baryons

In the minimal quark model, the baryon (anti-baryon) is a bound state of three quarks (anti-quarks). When baryon is formed in a particle reaction, an anti-baryon is simultaneously created. This process is explained by using a new quantum number called the baryon number $\mathcal{B}$. Baryons are assigned $\mathcal{B} = 1$ whereas anti-baryons $\mathcal{B} = -1$. Thus each quark (anti-quark) is assigned to have $+\frac{1}{3}(-\frac{1}{3})$ as baryon number. The value of this quantum number for all other particles is $\mathcal{B} = 0$. It is conserved in all particle decays and reactions.

Since the quarks are fermions, so the wave function of baryons must be anti-symmetric under the exchange of any two quarks. In SU(3) representation, three flavours *u, d,* and *s* make ordinary baryons. With these three flavours of quarks, the decomposition is:

$$3 \otimes 3 \otimes 3 = 10_S \oplus 8_M \oplus 8_M \oplus 1_A$$

The subscripts on the right side show that decuplet is symmetric in flavour, singlet is anti-symmetric and two octets have mixed symmetry [18]. The ground state baryons are shown in Figures 2.1 and 2.2 [19, 20].

In the ground state multiplets, the SU(3) singlet state is forbidden by Fermi Dirac statistics. The addition of fourth quark, the charm quark, extends the SU(3) symmetry to SU(4). However, due to heavy mass of charm quark, SU(4) symmetry is strongly broken than SU(3) of the light quarks. SU(4) multiplets made up of *u, d, s, and c* are shown in the Figure 2.3

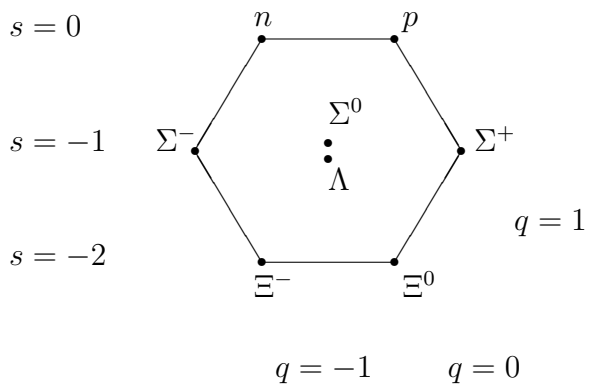

Figure 2.1: The baryon octet with spin 1/2 [19].

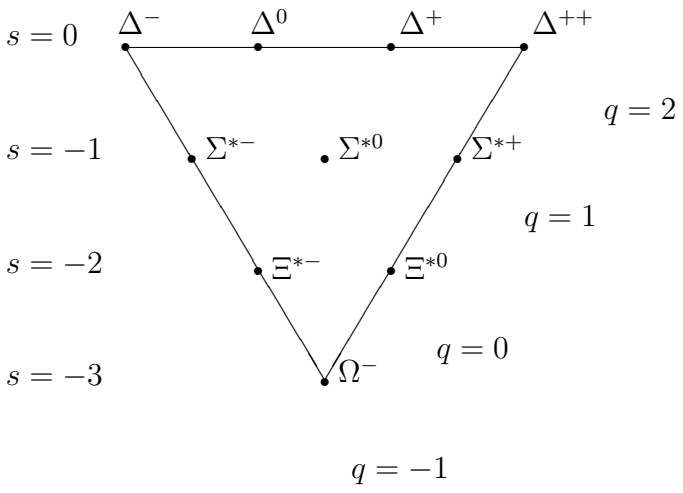

Figure 2.2: The baryon decuplet with spin 3/2 [19].

2.1.5 Mesons

Mesons are composed of a quark and anti-quark. As the quarks are spin half particles, so the total spin S of the mesons is either 0 or 1 i.e. mesons have integral spin. The total angular momentum J of the mesons is the vector sum of spin S and its angular momentum L i.e. J = L + S. In contrast to baryon number, there is no meson number associated with mesons [21, 22]. In SU(3) representation, there are nine possible states for the three light quark flavours (*u, d, and s*). They are grouped into an octet and singlet

$$3 \otimes 3 = 8 \oplus 1$$

By including charm quark also the SU(3) representation can be extended to SU(4). However the SU(4) symmetry is strongly broken due to heavy mass of charm quark. Nevertheless, in SU(4) representation, sixteen mesons are classified into a 15-plet and singlet.

$$4 \otimes 4 = 15 \oplus 1$$

Mesons are also classified in J^{PC} multiplets. The states with angular momentum L = 0 are pseudo-scalars with $J^{PC} = 0^{-+}$, and states with $J^{PC} = 1^{--}$ are vector mesons. For L = 1 the states are scalars with $J^{PC} = 0^{++}$, the axial vectors $J^{PC} = 1^{++}$ and $J^{PC} = 1^{+-}$ and the tensors with $J^{PC} = 2^{++}$. The ground state pseudo-scalars and vector mesons are shown in Figure 2.4

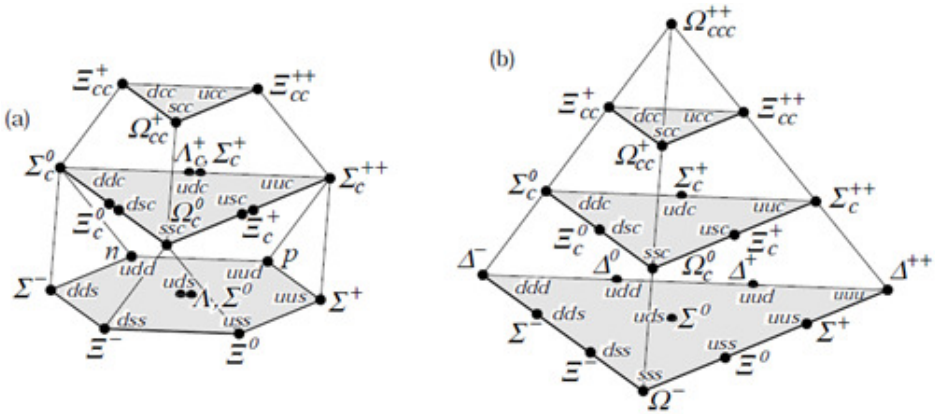

Figure 2.3: "SU(4) multiplet of baryons composed of *u, d, s* and *c* quarks. Figure(a) shows that 20-plet with an SU(3) octet and Figure(b) 20-plet with SU(3) decuplet" [21].

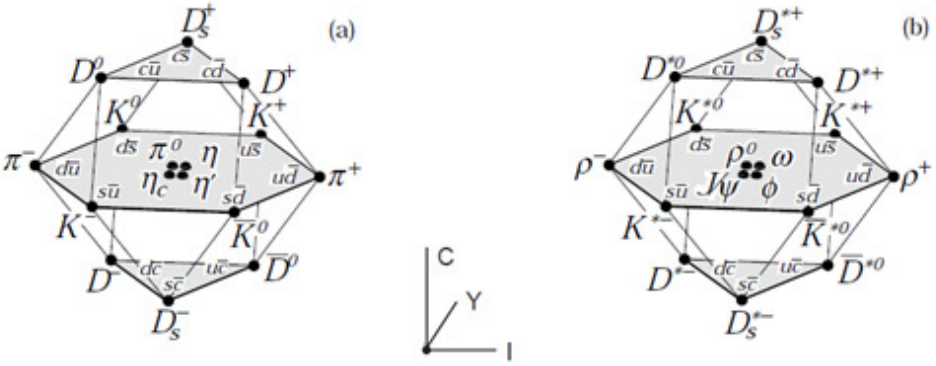

Figure 2.4: "The weight diagram for the ground state pseudoscalar mesons (a) and vector mesons (b) made of *u, d, s* and *c*quarks as a function of isospin I, charm and hyper charge" [21].

2.2 Fundamental Interactions

All the physical processes are based on four types of fundamental interactions: electromagnetic, weak, strong and gravity. The standard model describes all interactions except gravity. Leptons interact through only electromagnetic and weak forces. While quarks due to colour charge, interact in all three ways i.e. through electromagnetic, weak and strong forces. Corresponding to each interaction, there is a force carrier or mediator called gauge boson e.g. photons $W^{\pm}$ and Z^{o}. Electrically charged particles interact electromagnetically through exchange of photons. The weak force is mediated by $W^{\pm}$ and Z^{o} bosons. The strong force is mediated via exchange of gluons. Electromagnetic and weak forces have been unified into electroweak force which is studied in the framework of electroweak theory.

2.3 Symmetries and Conservation Laws

Symmetries play an important role in physics and are expressed by the invariance of physical laws with respect to some group of transformations either discrete or continuous [23]. If a system remain unchanged under a transformation of one or more variables, the system is said to have a symmetry under that transformation. Every symmetry of the nature is associated with some conservation laws e.g. translational invariance in space leads towards the conservation of linear momentum similarly the invariance under rotation yields the law of conservation of angular momentum [24, 25, 26].

2.3.1 Parity

Parity is an intrinsic property of all fundamental particles. In quantum mechanics, this property is defined in terms of parity operator P, which is related to orbital angular momentum L by the relation:

$$P = (-1)^{L+1}$$

where L is restricted to integral values. Mathematically, this operator is defined as the inversion of the spatial coordinates $x \rightarrow -x$. It is odd (-1), if a wave function changes the sign under parity operation, and is even (+1), if it remains unchanged. The parity operator is multiplicative i.e. parity of a composite state is equal to the product of parities of its constituents. It is conserved in strong and electromagnetic interactions. By convention, quarks (fermions) have positive parity and anti-quarks (anti-fermions) have negative parity [27, 28].

2.3.2 Charge Conjugation

The charge conjugation C, is an operation that changes the particles to anti-particles. This operation reverses all the internal quantum numbers (charge, baryon number, lepton number, strangeness and other flavours etc.) but the mass, energy, momentum and spin remain unchanged. Like parity operator charge conjugation too has got unit value with ± signature. For fermion-antifermion bound state, the charge conjugation parity (C-parity) is defined

as

$$C = (-1)^{L+S}$$

where L and S are the orbital angular momentum and total spin respectively. Except weak interactions, it is conserved in strong, electromagnetic and gravitational interactions [29].

2.3.3 Isospin

The concept of isospin is similar to that of angular momentum. This appear as a result of slight difference in the masses of proton and neutron. They both form an isospin doublet with isospin quantum number I = 1/2, with third component of isospin I_3 having the values of 1/2 and -1/2 for proton and neutron respectively. It is of great importance for the classification of observed particle families. We can describe the isospin multiplets in analogy with the angular momentum and spin multiplets. Similarly the pions (π^+, π^- and π^o) have isospin quantum numbers I = 1, thus the corresponding I_3 values are 1, 0 and -1 for π^+, π^0 and π^-respectively [30].

Table 2.2: The values of $\mathcal{B}$, Y, Q and I and I_3 involves in our work

Particles	$\mathcal{B}$	Y	Q	I	I_3
π^+	0	0	1	1	1
π^-	0	0	-1	1	-1
Λ	1	0	0	0	0
p	1	1	1	1/2	1/2

There are some other important quantum numbers conserved in strong interactions like Hypercharge Y and electric charge Q, which are related by

Gell-Mann-Nishijima relationship

$$Q = I_3 + \frac{Y}{2}$$

where

$$Y = \mathcal{B} + S + C + B + T$$

In above expression, $\mathcal{B}$ is the baryon number, S is strangeness, C is charmness, B is bottomness and T is the topness quantum numbers. The electric charge is related to isospin by By convention, the flavour of quark has the same value as its charge Q. The values of baryon numbers $\mathcal{B}$, Hypercharge Y, charge Q and Isospin I and third component of isospin I_3 are listed in table for some isospin multiplets involved in our work.

2.4 Charmonium

In November, 1974, the discovery of an unusual resonance opened a new era in the field of high energy physics. This new resonance was discovered independently by two different experimental groups at Brookhaven National Laboratory (BNL) and Stanford Linear Accelerator (SLAC). At BNL, the group led by Ting reported the observation of heavy particle in the mass spectrum of of e^+e^- near the energy of $3.1GeV/c^2$. It was observed at $30GeV$ in the following reaction:

$$p + Be \rightarrow e^+ + e^- + x$$

[5]. The SLAC group led by B. Richter observed a very sharp peak at the centre of mass energy of $3.1 GeV/c^2$ in the following reaction:

$$e^+e^- \rightarrow hadrons, e^+e^- and \mu^+\mu^-$$

[6]. The BNL group called this particle J whereas the SLAC group called this particle ψ and thus known as J/ψ. Soon after the discovery of J/ψ, the preliminary results were reported for the confirmation of newly discovered particle in the e^+e^- annihilation experiments at Frascati [31]. Further it was confirmed by DASP collaboration in the elastic scattering of e^+e^- at DESY[32].

After the discovery, much theoretical efforts have been made for the interpretation and decay properties of J/ψ resonance. The charmonium model [33] - [42] interprets this resonance as the bound state of a new flavour of quark, the charm quark and charm anti-quark ($c\bar{c}$). The idea of charm quark had already been introduced by S. L Galshow and Yasuo Hara in 1964 to construct a symmetry between four quarks and four leptons [43, 44, 45] . M. K. Gaillard and B. W. Lee suggested the mass of charm quark [46]. The interpretation of J/ψ as a $c\bar{c}$ bound state received a strong support from the observation of charmed meson [47].

Further evidences for the interpretation of J/ψ as $c\bar{c}$ bound state follows from narrow widths which were determined to be < 100 KeV. For a state which decays to hadrons by strong interaction, is expected to have width in MeV. But J/ψ width is three times smaller than the expected width if it were composed of uncharmed quark and antiquark [48]. The small width of J/ψ

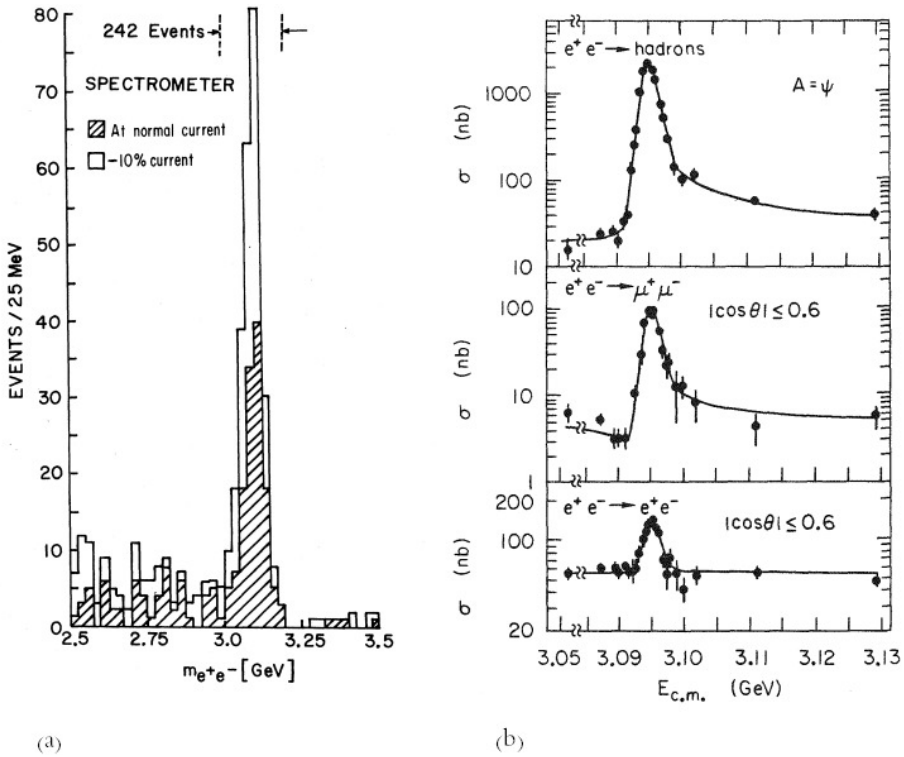

Figure 2.5: (a) "The narrow resonance peak of J/ψ in the invariant mass distribution of e^+e^- produced in the reaction $p + Be \to e^+ + e^- + x$ at BNL"[5].
(b) "The observation of J/ψ at $3.1 GeV/c^2$ in the cross section of e^+e^- for various decay channel, showing the sharp peak and narrow width of J/ψ resonance" [6].

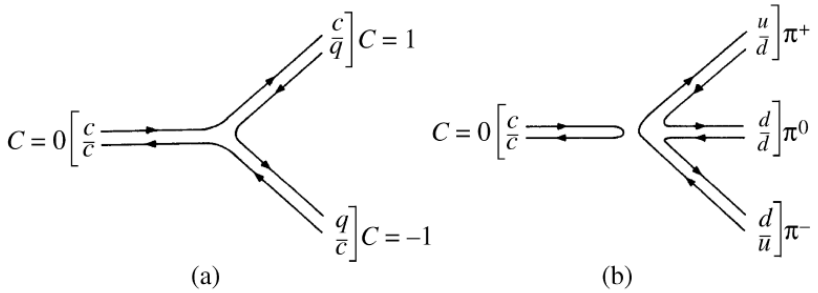

Figure 2.6: "(a) OZI allowed and (b) suppressed process of charmonium." [48]

is attributed to OZI rule (Okubo, Zweig, Iizuka) [49, 50, 51]. The OZI rule states that the strong decay processes, in which the initial quark pairs do not appear as final quark pairs, are strongly suppressed. More simply this rule tells that, the strong processes, described by Feynman diagrams containing detached quark line are strongly suppressed as compared to the diagrams in which quark line are connected [52]. Figure 2.6 (a) and (b) describe the OZI allowed and suppressed decays of charmonium state respectively [53]. The detached quark line in the initial and final states requires to be connected through gluons. Since the decaying particle is a colour singlet vector meson, two gluons are required for colour conservation while charge parity is odd and demands exchange of three gluons. [54, 55].

Shortly after the discovery of J/ψ, SLAC group discovered another narrow resonance, $\psi(2S)$ at the centre of mass energy just below 3.7 GeV in the cross section of $e^+e^- \rightarrow hadrons$ [7]. After that another resonance, $\psi(3S) or \psi''$ at 3.77 GeV, was found by DASP collaboration [56]. It was concluded that these resonances are composite state of charm-anticharm quark also known as *charmonium*.

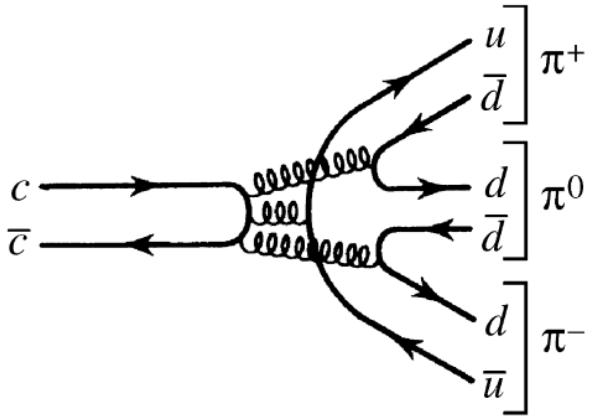

Figure 2.7: "OZI suppressed process of charmonium".[48]

2.4.1 Charmonium Spectrum

Later on, more charmonium states were observed experientially, further conforming the existence of charm quark [57, 58, 59]. The observed charmonium states are shown in Fig.2.8. The charmonium states or energy levels are described with spectroscopic notation $n^{2S+1}L_J$ where L is the orbital angular momentum, S is spin of the quark and anti-quark and J total angular momentum and "n" represents the radial excitation number. Since quarks are fermion (spin-1/2 particles), the total spin takes the values of 0 and 1, and comes out four possible spin states of $c\bar{c}$ pair i.e into a singlet and a triplet state [60]. The radial excitation of $c\bar{c}$ result in a spectrum having same values of S, L and J corresponding to different radial excitation number "n". For example for n=1 with L=0 and S =0 the state is represented as 1^1S_0 which is the lowest state and for n=2 with same L and S, the state is 2^1S_0. Similarly for n=1 with L=0 and S =1 the state is represented as 1^3S_1 which is the lowest state and for n=2 with same L and S, the state is 2^3S_1.

The charmonium states can also be described in term of J^{PC}, where P

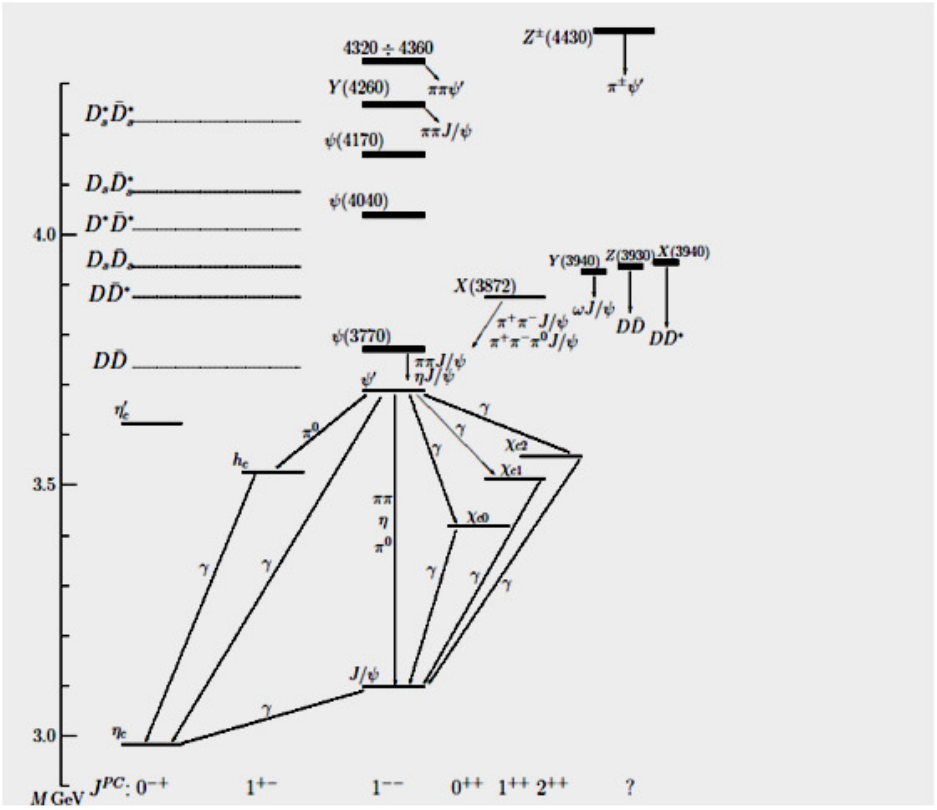

Figure 2.8: The charmonium and its related resonances and transitions between different states. The states are labelled with spectroscopic notation $n^{2S+1}L_J$, where n is the principal quantum number, S represents the spin of the particle and S = 0, 1, L = S, P, D, ... denotes the orbital angular momentum of L = 0, 1, 2, ..., and J is the total angular momentum. In addition to this notation, parity (P) and charge conjugation (C) are used in the notation J^{PC}. Dotted line shows the threshold for various charmed meson [60].

is the parity and C is the charge conjugation. For quark anti-quark bound system the $C = (-1)^{L+S}$ and $P = (-1)^{L+1}$. Therefore the $^1S_0$ states have $J^{PC} = 0^{-+}$ and $^3S_1$ states have $J^{PC} = 1^{--}$. The lowest energy states for mesons with quark-antiquark pairs have spin S = 0 and negative parity are called pseudo-scalar mesons, e.g. $\eta_c(1S)$ and $\eta_c(2S)$. For excited states of mesons the quark spins are parallel, so if a state has zero orbital angular momentum, then the total angular momentum of the particle is 1. Such states are called vector mesons, e.g. J/ψ and $\psi(2S)$.

More detailed descriptions and discussion about Charmonium can be found in Ref.[61] and [62].

2.4.2 Production and decay mechanisms of charmonium

Most of the charmonium spectroscopy was carried out in e^+e^- collision experiments in which e^+e^- may annihilate through virtual photon and creats a $c\bar{c}$ bound state, as shown in the Fig.2.9. As the vector mesons have quantum

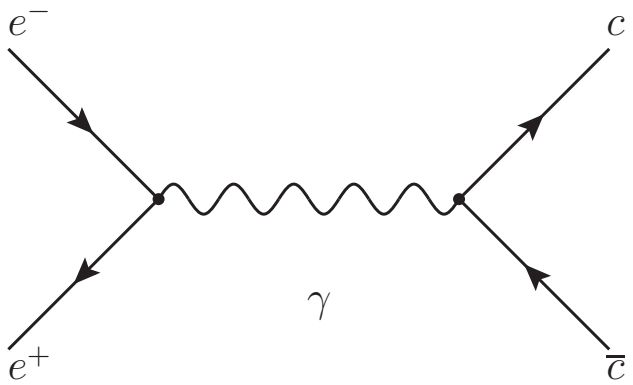

Figure 2.9: Feynman diagram for the production of $c\bar{c}$ in e^+e^- process[63].

numbers $J^{PC} = 1^{--}$, same as that of photon, they can be produced directly in e^+e^- collisions, in which virtual photons are formed. The $c\bar{c}$ bound states can also be produced in e^+e^- collision in the initial state radiation (ISR) processes in which, either the electron or positron radiates a photon and then annihilate, thereby lowering the effective centre of mass energy. This is very useful process for searching new vector mesons. In B meson decay, charmonium state of any quantum number can be produced. The annihilation of $p\overline{p}$ makes it possible to study the full charmonium spectrum [63].

The charmonium states can decay through electromagnetic or hadronic processes involving the radiative transition or annihilation decays as shown in Fig.2.10. The radiative transitions have mainly tow types: electromagnetic and hadronic. Electromagnetic transitions involves the decay of charmonium states to their low lying charmonium states by emitting photons. In hadronic transitions, charmonium states are converted into lower states via emission of lighter mesons. The annihilation decays are of two types: hadronic and electromagnetic. In hadronic annihilation of charmonium , the charm-anticharm quark pair annihilate into three gluons which in turn produced hadrons. The hadronic decay modes of $\psi(2S)$ are strongly suppressed in accordance with OZI rule. Due to this strong suppression, the probability electromagnetic decays of $\psi(2S)$ become comparable with that of hadronic decays [64]. That's why its leptonic decays have significant branching fraction. In electromagnetic annihilation, the the hadrons are produced from the photons created due to annihilation of charm-anticharm quark pair. The annihilation decays are mainly divided into two or three body intermediate state decay processes. Two body decays involve a meson pair or baryon anti-baryon pair. Three

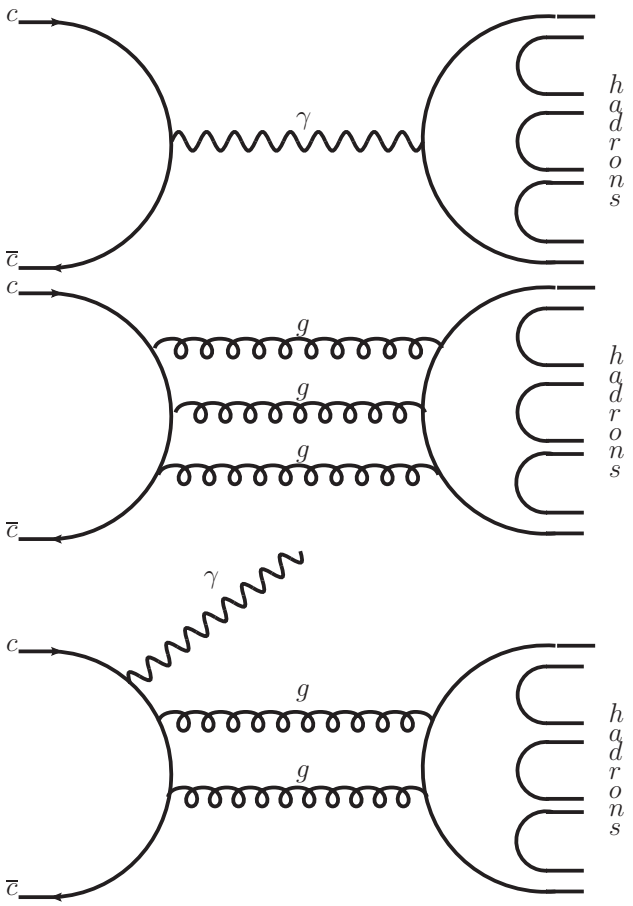

Figure 2.10: Charmonium decays via one photon, via three gluons and via one photon and two gluons [64].

body decay may involve three meson or a baryon anti-baryon pair accompanied by a meson. These decay modes provide excellent opportunities to search for hybrids, study light hadron properties, investigate excited states, search for glueballs, probe the possibility of the decay processes violating conservation laws such as lepton flavour number, isospin, C-Parity, strangeness, etc. [65].

Chapter 3

Experimental Setup

3.1 Beijing Electron Positron Collider II (BEPC II)

[1]The upgraded Beijing Electron Positron Collider II is a two ring, multi bunch collider with designed luminosity of $10^{33}cm^{-2}s^{-1}$ at center of mass energy of 3.78 GeV. It is designed to operate in τ charm energy region ($\sqrt{s} = 2.0 - 4.6GeV$) [66]. The two rings are used to store the electron and positron beams separately. There are 93 bunches in each ring with bunch spacing of 8ns. The electron and positron beam current is 0.91A and the electron injection rate is 200mA/min and that of positron is 50 mA/min. The electron positron beams collides head on at the interaction point with horizontal crossing angle of ± 11 mrad [67].

The major components of collider are injection kickers, beam control op-

[1] "The material presented in this chapter has been taken from scholarly work whose references are given. Author has no intention to own any material reported without references"

tics, RF cavities, beam pipes, vacuum system, superconducting quadruple magnets, power supplies and beam instrumentation and control [68].

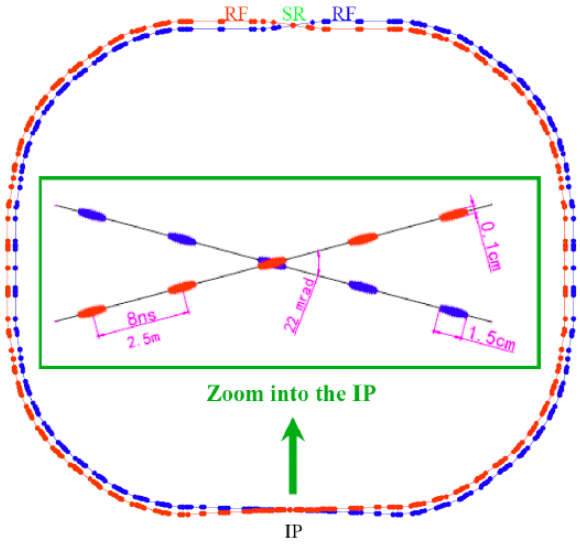

Figure 3.1: A sketch of Beijing Electron Positron Collide II (BEPC II). The interaction point is shown with crossing a crossing angle of $\pm 11 mrad$ and bunch spacing of 8ns.

3.2 The Beijing Spectrometer III (BES III)

The Beijing Spectrometer III, as shown in Fig.3.2, is a detector to perform experiments at BEPC II. It consists of Main Drift Chamber (MDC), Time of flight, Electromagnetic calorimeter and Muon identifier.

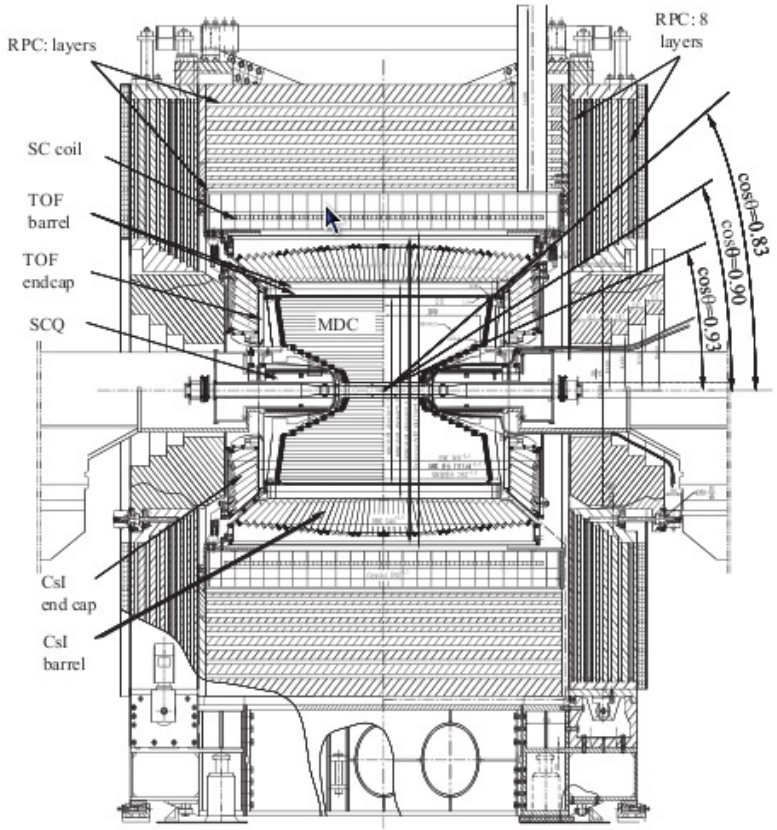

Figure 3.2: Schematic diagram of BES III detector [68].

3.2.1 Main Drift Chamber (MDC)

Main Drift Chamber (MDC) is one of the most important and innermost component of BES III detector. It is used to measure the momentum of the charge particle and energy loss per unit length for particle identification. In order to minimize the effect of multiple scattering, a Helium based gas mixture ($He-C_3H_8$) in the ratio of 60:40 is chosen as working gas. The inner and outer radius of MDC are 59 mm and 810 mm respectively. The polar angle coverage of MDC is $\mid \cos\theta \mid < 0.93$. MDC has 43 cylindrical layer of small drift cells that are coaxial with beam pipe. Aluminum and gold plated

tungsten wire are used for the field shaping and for signals respectively. The single wire resolution is better than 130μm in r-ϕ plane and the position resolution in the z-direction (beam direction) at the vertex is expected to be 2mm. The expected transverse momentum resolution is 0.5% at 1GeV/c in 1T magnetic field [69]. Fig.3.3 shows the schematic view of MDC.

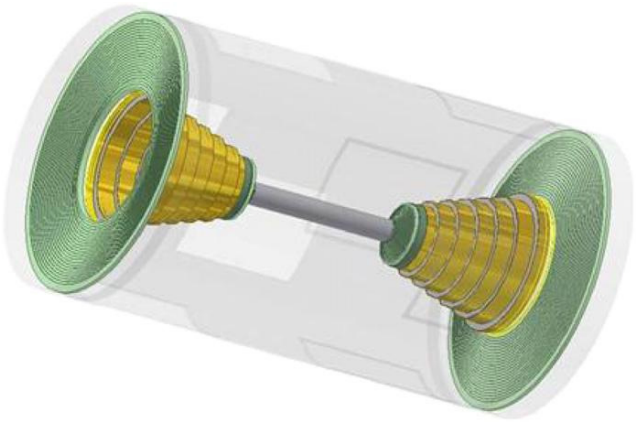

Figure 3.3: A schematic view of Main Drift Chamber of BES III [67].

3.2.2 Time of Flight System (TOF)

This system is used to measures the time of flight of charged particles for their identification. It also plays an important role as fast triggers for charged

particles and helps to suppress backgrounds from cosmic rays. TOF system based on plastic scintillator bars and read out by fine mesh photo-tubes. It consists of a barrel and two end caps. The barrel TOF covers the solid angle $|\cos\theta| < 0.83$ and for end cap its value is $0.85 < |\cos\theta| < 0.95$. The barrel TOF has two layers having 88 scintillating bars. Each bar has a thickness of 50mm and is read out at each end by fine mesh photo-multiplier tubes(PMT). Each single layer end cap TOF have 48 fan shaped counters. These end caps TOF are located out sides MDC end caps. The expected time resolution for TOF is 100ps.

3.2.3 Electromagnetic Calorimeter (EMC)

The EMC is comprised of 6240 CsI(TI) crystals, designed to measures the energies and positions precisely. It consists of one barrel and two end cap [71].

- The EMC barrel has inner radius of 940mm with angular coverage of $|\cos\theta| < 0.82$.
- There are 44 crystal rings in the EMC barrel, each has 120 crystals.
- The end caps have inner radius of 500mm and covers the polar angle range $0.83 < |\cos\theta| < 0.93$.
- Each endcap comprises of 6 rings that are split into two tapered half cylinder.

The designed energy resolution electromagnetic calorimeter is $\sigma_E/E = 2.5\%$ at 1GeV and position resolution of $\sigma_{xy} = 6mm/\sqrt{E}$ where E is in

Table 3.1: Designed Parameters of BEPC II [68]

BEPC II parameters	Designed Values
Center of mass energy region	2.0 - 4.6 GeV
Number of rings	2
Circumference	237.5
luminosity at 3.78GeV	$10^{33} cm^{-2} s^{-1}$
Number of bunches in each ring	93
Relative energy spread	5.16×10^{-4}
Crossing angle	$\pm$11mrad
Beam current	2$\times$0.91A
Electron injection rate	200 mA/min
Positron injection rate	50mA/min

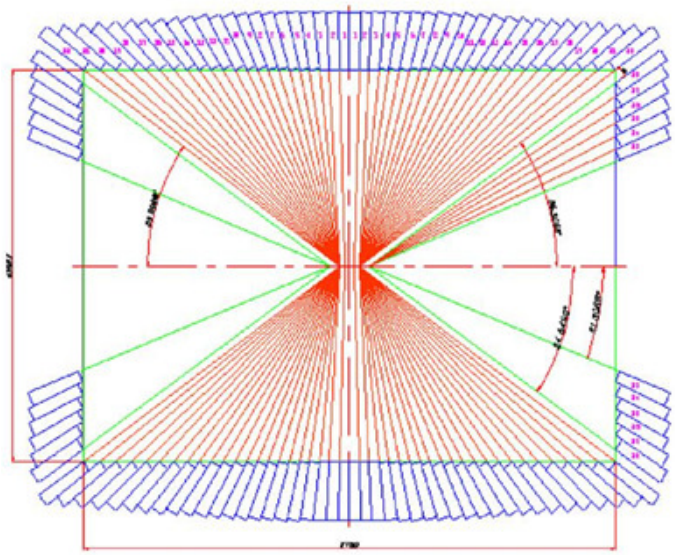

Figure 3.4: Schematic view of Electromagnetic Calorimeter.

GeV.The total weight of crystals is 25.6 tons.

3.2.4 Muon Identifier

The BES III muon identifier is made of resistive plate chambers (RPC). The basic function of muon identifier is to differentiate muons from hadrons by their hit patterns in the magnetic flux return yoke.

3.3 Super-conducting magnet

The BES III super-conducting solenoid magnet (SSM)of radius of 1.48m and length of 3.52m, use Al stabilized NbTi/Cu conductor. Its coil has 920 turns and is situated outside EMC. A stable magnetic field of 1.0 Tesla is achieved by SSM.

3.4 Trigger System

The latest technology based BES III trigger system has expected trigger rate of 4KHz. The trigger system consists of two level. Hardware trigger level (Level 1) and software trigger level (L2). Information from different sub-detector electronics is transported into sub-trigger system via optical fiber to generate trigger condition. The trigger and other related conditions are generated by using information from trigger signals of TOF, MDC and Electromagnetic Calorimeter (EMC). Global trigger logic is employed by Level 1 sub-triggers.

3.5 Detector Control System

The Detector Control system (DCS)[70] is the most important system of BES III. Its main task is to monitor and control the status of accelerator and spectrometer. It also monitor the status of the sub-detectors, readout electronics, the PC farms, the environmental conditions like temperature and humidity and radiation level etc. The DCS consists of six subsystems:

- "Temperature and Humidity (TH) Monitoring System",
- "Low-voltage (LV) Power Supply Monitoring system",
- "High-voltage (HV) Power Supply Monitoring and Control System",
- "VME Crates Monitoring and Control System",
- "Gas Control System"
- "Safety interlocking (SI) System" among the detector system.

The DCS is organized into three layers

- "Front End layer" (FEL)
- "Local Control Layer" (LCL)
- "Global Control Layer" (GCL)

Simple sensors, computerized devices and programmable logical controllers (PLC) are used in the FEL to collect data. The FEL transported this data to LCL. LCL offers monitory and control functions such as displaying, archiving and alert handling. "In the GCL, the global control station (GCS) will

accumulate the summary information from LCL and provide a uniform and simple interface to operators for the overall monitoring and control of the whole BES III experiment. All the information acquired by the LCS will be stored in a database and published to Internet by the web server. The GCL work in integrated mode during concurrent physics data taking while local control station (LCS) can work either in stand-alone mode or integrated mode according to requirement of different stages of experiment" [70].

3.6 Physics Studies at BES III

The Physics program at BES III provides an excellent opportunity to improve the understanding of Standard Model processes and as well as physics beyond the Standard Model. This program includes the study of light hadron spectroscopy, electroweak physics, QCD, τ-physics, Charm physics, properties of charmed mesons and baryons, measurement of CKM and QCD parameters, glueballs search, exotic and multi-quark states, search for new physics, etc.

Table 3.2: Parameters of BES III. [68]

Subdetector	Parameter	Values
MDC		
	single wire resolution	$\sigma = 130\mu m$
	Number of rings	2
	momentum resolution	$\sigma_p/p = 0.5\%$
	dE/dx resolution	$\sigma(dE/dx) = 6\%$
TOF		
	Time resolution	$(\sigma T)_{barrel} = 100ps$
		$(\sigma T)_{endcap} = 110ps$
EMC		
	Energ resolution	$\sigma E/E = 2.5\%$at 1GeV
	position resolution	0.6cm
Muon Identifier		
	No. of layers(barrel)	9
	No. of layers(endcap)	8
	Cut-off momentum	0.4MeV/c
Super-Conducting Magnetic field	1.0T	

Chapter 4

Measurement of $\psi(2S)$ decays into $\Lambda\overline{\Lambda}\pi^+\pi^-$

4.1 Introduction

The charmonium states J/ψ and its first excited state $\psi(2S)$ are the non-relativistic bound states of charm-anticharm ($c\bar{c}$) quarks. These states predominantly decay to light hadrons either via annihilation into three gluons or single photon. The annihilation of charmonium state is ideal to study light hadron spectroscopy and their production mechanism. Since the discovery of charmonium states, many experiments are being conducted in different high energy physics labs. In this regard, huge data collected at BES III, gives an excellent opportunity to access small branching fractions and precise measurements of previously studied decay channels of J/ψ and $\psi(2S)$. The branching fraction of the decay channel $\psi(2S) \to \Lambda\overline{\Lambda}\pi^+\pi^-$ has already been measured in CLEO experiment using $3.08 \times 10^6 \psi(2S)$ events

[77] . Our analysis is based upon 106×10^6 $\psi(2S)$ data sample, collected at BES III. We report the improved branching fractions of $\psi(2S) \to \Lambda\bar{\Lambda}\pi^+\pi^-$, $\psi(2S) \to \Xi^-\bar{\Xi}^+$ and $\psi(2S) \to \Sigma^{*+}\bar{\Sigma}^{*-}$ to be $(1.34 \pm 0.05_{stat} \pm 0.24_{sys}) \times 10^{-4}$, $(3.15 \pm 0.35_{stat} \pm 0.55_{sys}) \times 10^{-5}$ and $(3.39 \pm 0.34_{stat} \pm 0.61_{sys}) \times 10^{-5}$, respectively. The analysis is explained in following sections.

4.2 Data samples, software framework and BOSS Version

4.2.1 Data Samples

This analysis is performed using the following data samples

- 1.06×10^8 $\psi(2S)$ data events accumulated at BES III in April 2009 [72].
- 1.0×10^5 Monte-Carlo sample.
- 1.06×10^8 inclusive Monte Carlo sample.

4.2.2 Software framework and BOSS version

The Monte-Carlo simulation is used to determine the detection efficiency, optimization of event selection and for the estimation of the possible background. A GEANT 4 based [73, 74] BES III Object Oriented Simulation Tool (BOOST) is used for the simulation of the detector. It includes the geometry and material descriptions of the BES III detector. This analysis is

performed using BES III Offline Software System (BOSS)[75] which is based upon Gaudi [76]. We used BOSS 6.5.5 for our analysis.

4.3 Event Selection

The decay mode $\psi(2S) \to \Lambda\overline{\Lambda}\pi^+\pi^-$ is studied with the following selection criteria.

4.3.1 Initial Event Selection

1. good charged track selection

    - The charged tracks are reconstructed from MDC with good helix fit.
    - $\mid V_z \mid < 15cm$ and $\mid V_{xy} \mid < 10cm$ here $\mid V_z \mid$ and $\mid V_{xy} \mid$ are the nearest distance to interaction point in z-direction and xy-plane.
    - selection of charged tracks satisfying $\mid \cos\theta \mid \leq 0.93$ where θ is the polar angle between the charged track direction and beam direction.
    - Each charged track is required to have transverse momentum satisfying $P_{xy} > 0.05$
    - There are two protons and four pions in the final state. So number of good charged tracks satisfying the above criteria is required to be six with net charge zero.

2. Particle Identification

- The dE/dx and TOF(Endcap and Barrel) information is used to identify proton and anti-proton.
- For identification of $p/\overline{p}$, it is requred that $Prob(p) > Prob(k)$ and $Prob(p) > Prob(\pi)$

3. Vertex Fitting

- A vertex fit is performed to one proton and negative charged tracks (π^-) assuming that they are originated form the interaction point
- we reconstruct a candidate Λ from the combination of $p\pi^-$
- by comparing χ^2 value, we select the right π^- for Λ.
- for events more than one Λ candidate, the one with least χ^2 is chosen.
- same method is applied for $\overline{\Lambda}$ selection.

4. 4-C Kinematic Fit

- The 4-C kinematic fit is applied to all candidiates satisfying $\psi(2S) \rightarrow \Lambda\overline{\Lambda}\pi^+\pi^-$ hypothesis by imposing four momentum conservation. Event with $\chi^2_{4C} < 100$ are selected.

The χ^2_{4C} distributions, invariant mass distributions of $p\pi^-$ and $\overline{p}\pi^+$ after initial event selection criteria are shown in Figures 4.1, 4.2 and 4.3 from MC and 4.4, 4.5 and 4.6 from data.

4.3.2 Final Event Selection

After initial event selection, the final event selection is listed below

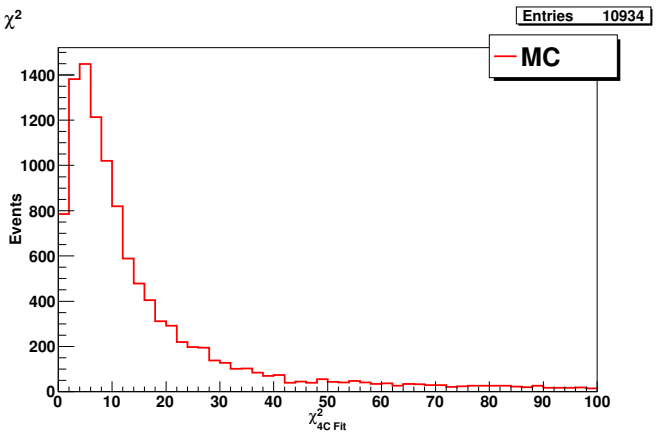

Figure 4.1: Distribution of χ^2_{4C} after initial event selection.

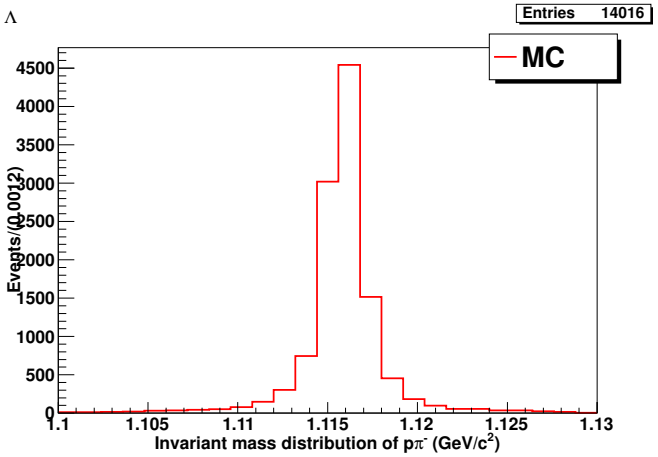

Figure 4.2: Invariant mass distribution of $p\pi^-$ for Λ after initial event selection.

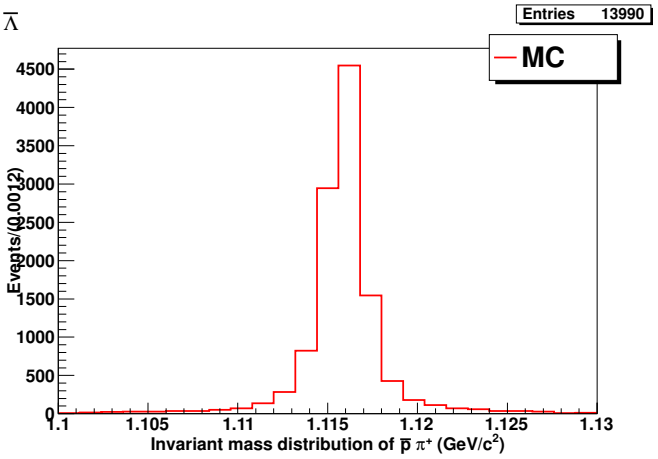

Figure 4.3: Invariant mass distribution of $\overline{p}\pi^+$ for $\overline{\Lambda}$ after initial event selection.

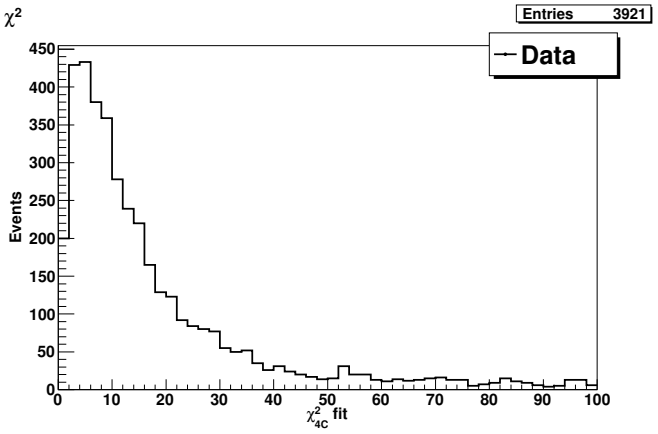

Figure 4.4: Distribution of χ^2_{4C} after initial event selection.

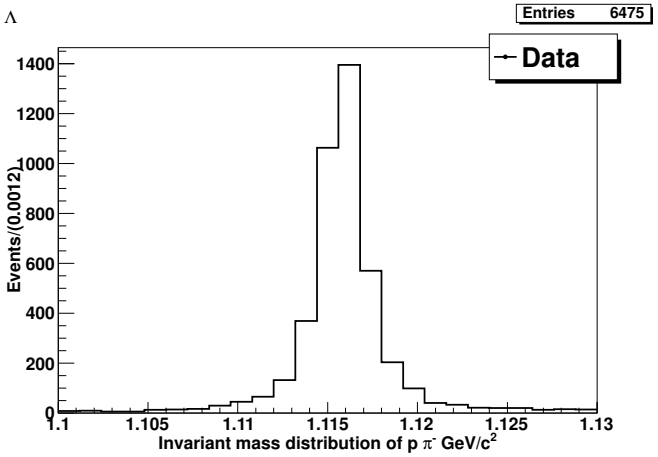

Figure 4.5: Invariant mass distribution of $p\pi^-$ for Λ after initial event selection.

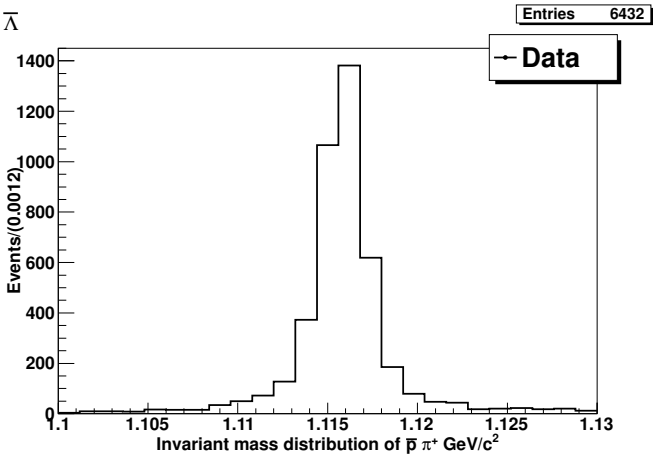

Figure 4.6: Invariant mass distribution of $\overline{p}\pi^+$ for $\overline{\Lambda}$ after initial event selection.

1. Mass Window cut

   - Λ and $\overline{\Lambda}$ mass constriants:
   - The final $p\pi^-$ invariant mass distribution is obtained after applying the mass constraints $\mid M_{\overline{p}\pi^+} - M_{\overline{\Lambda}} \mid < 0.005 GeV/c^2$
   - The final $\overline{p}\pi^+$ invariant mass distribution is obtained after applying the mass constraints $\mid M_{p\pi^-} - M_{\Lambda} \mid < 0.005 GeV/c^2$

2. χ^2 cuts for primary and secondary fits

   - To improve the resolution of $\Lambda/\overline{\Lambda}$, primary and secondary vertex fits are used successfully and to supress the backgound $\chi^2 < 1000$ for primary vertex fit $\chi^2 < 500$ for secondary vertex fits are used.
   - the decay lengths (DL) for reconstructed Λ and $\overline{\Lambda}$, $DL_{\Lambda/\overline{\Lambda}} > 0.005m$ is used for selection of events.

   After applying above event selection criteria, and following mass cut the plots of invariant mass distributions of $\pi^-\Lambda$ and $\pi^+\overline{\Lambda}$(Fig. 4.7), $\pi^+\Lambda$ and $\pi^-\overline{\Lambda}$(Fig. 4.8) and $\Lambda\overline{\Lambda}$ and $\pi^+\pi^-$(Fig. 4.9) are shown.

   (a) $\mid M_{\overline{p}\pi^+} - M_{\overline{\Lambda}} \mid < 0.005 GeV/c^2$

   (b) $\mid M_{p\pi^-} - M_{\Lambda} \mid < 0.005 GeV/c^2$

   (c) $DL_{\Lambda/\overline{\Lambda}} > 0.005m$

   (d) $\chi^2 < 1000$

   (e) $\chi^2 < 500$

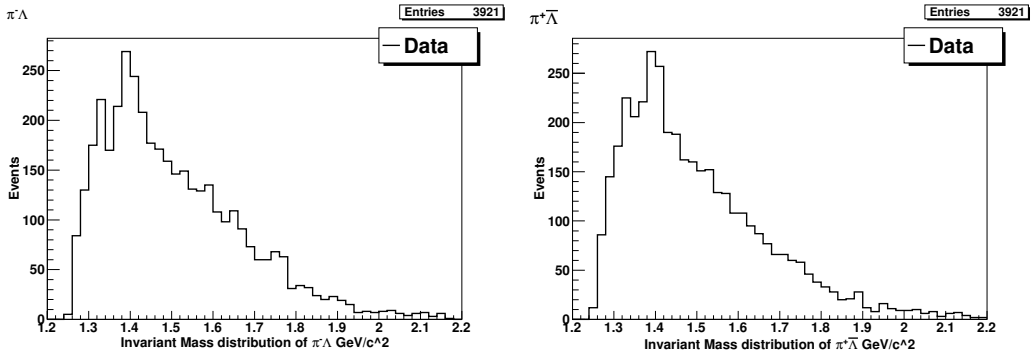

Figure 4.7: Invariant mass distribution of $\pi^-\Lambda$ (left) and $\pi^+\overline{\Lambda}$(right) after initial selection criteria.

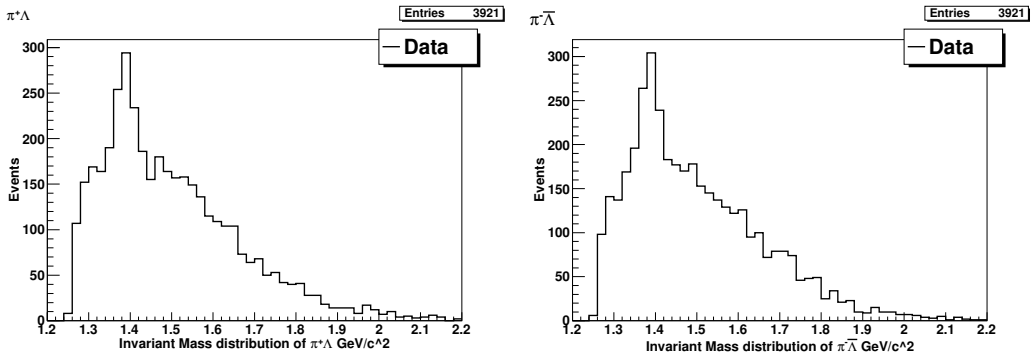

Figure 4.8: Invariant mass distribution of $\pi^+\Lambda$ (left) and $\pi^-\overline{\Lambda}$(right) after initial selection criteria.

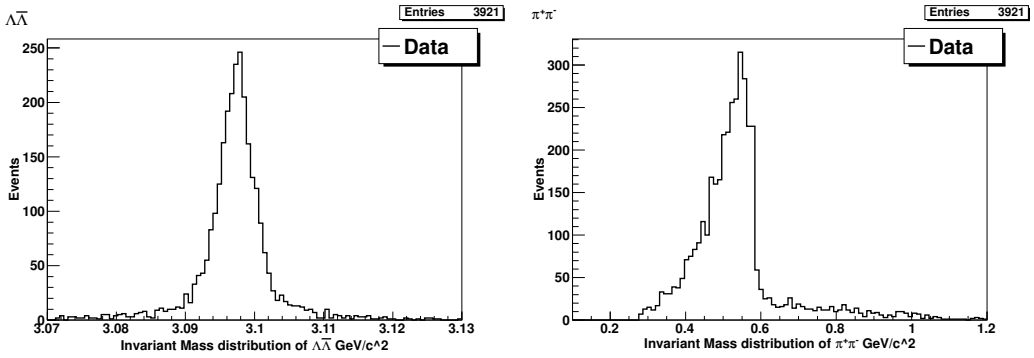

Figure 4.9: Invariant mass distribution of $\Lambda\overline{\Lambda}$ (left) and $\pi^+\pi^-$(right) after initial selection criteria.

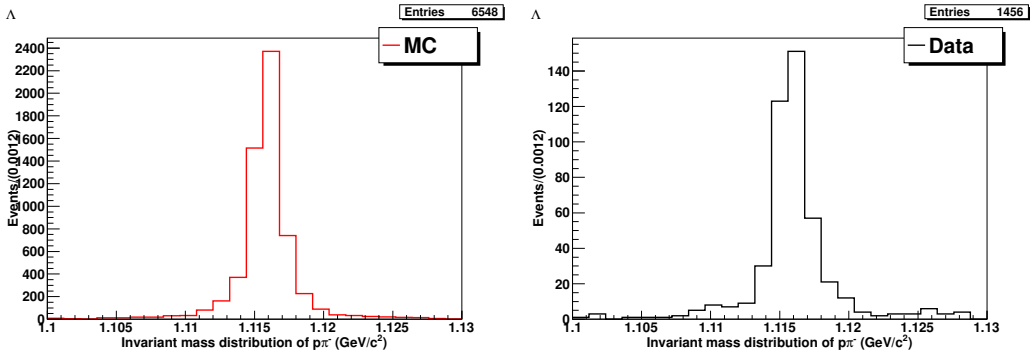

Figure 4.10: Invariant mass distribution of $p\pi^-$ for Λ after final event selection.

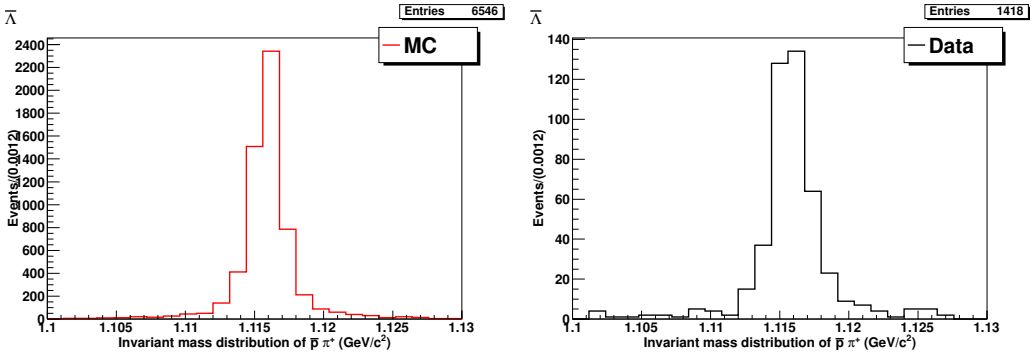

Figure 4.11: Invariant mass distribution of $\overline{p}\pi^+$ for $\overline{\Lambda}$ after final event selection.

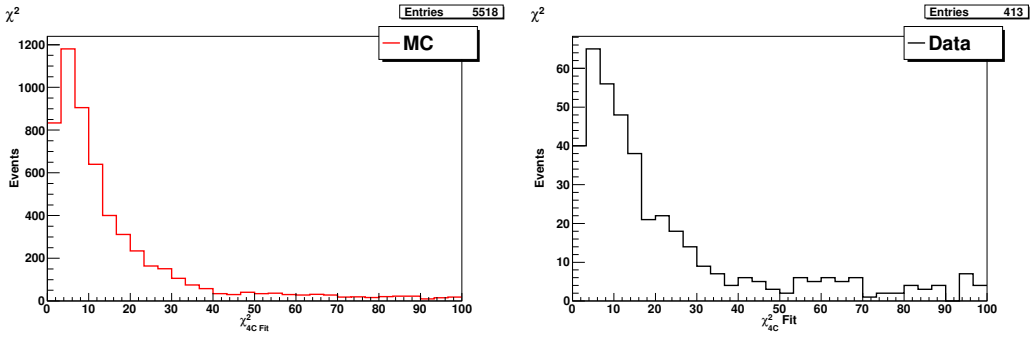

Figure 4.12: χ^2_{4C} distribution after final event selection.

3. reject Ξ^- and $\overline{\Xi}^+$:

   The invariant mass distribution of $\pi^-\Lambda$ and $\pi^+\overline{\Lambda}$ in data is shown figure 4.7. The Ξ^- and $\overline{\Xi}^+$ signals are clear near $1.321GeV/c^2$. Σ^{*-} and $\overline{\Sigma}^{*+}$ peaks are also clear. These background events contributions are from $\psi(2S) \to \Xi^-\overline{\Xi^+}$. We apply the mass constraint of $\mid M_{\pi^-\Lambda} - M_{\Xi^-} \mid > 0.013GeV/c^2$ and $\mid M_{\pi^+\overline{\Lambda}} - M_{\overline{\Xi}^-} \mid > 0.013GeV/c^2$.

4. reject Σ^{*+} and $\overline{\Sigma}^{*-}$:

   The invariant mass distributions of $\pi^+\Lambda$ and $\pi^-\overline{\Lambda}$ are shown in Fig. 4.8, Σ^{*+} and $\overline{\Sigma}^{*-}$ signals are clear, To reject this events we use mass constraints of $\mid M_{\pi^+\Lambda} - M_{\Sigma^{*+}} \mid > 0.09GeV/c^2$ and $\mid M_{\pi^-\overline{\Lambda}} - M_{\overline{\Sigma}^{*+}} \mid > 0.09GeV/c^2$.

5. reject J/ψ

   J/ψ peak is clear in the invariant mass distribution of $\Lambda\overline{\Lambda}$, the J/ψ events candidates are from $\psi(2S) \to J/\psi\pi^+\pi^-$, $J/\psi \to \Lambda\overline{\Lambda}$, so the events around J/ψ paek are rejected by using the cut $\mid M_{(\Lambda\overline{\Lambda})} - M_{J/\psi} \mid > 0.009GeV/c^2$

6. $\pi^+\pi^-$ mass constriant:

   The invariant mass distribution of $\pi^+\pi^-$ is shown in the Fig.4.9 which shows a clear signal of ρ_0. These background events are from the $\psi(2S) \to \overline{\Lambda}\rho_0\Lambda$. In order the eliminate these background events we apply the the following mass cut of $\mid M_{\pi^+\pi^-} - M_{\rho_0} \mid > 0.009GeV/c^2$.

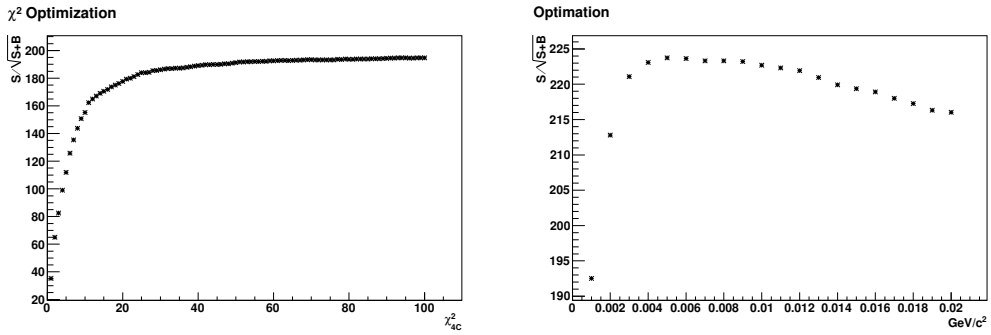

Figure 4.13: Optimization of χ^2_{4C} and $\Lambda/\overline{\Lambda}$ cuts.

4.4 Optimization

In order to suppress the background and to increase the ratio of signal to square root of signal plus background i.e. $\frac{S}{\sqrt{S+B}}$, we optimized the mass cut for Λ and $\overline{\Lambda}$ and χ^2_{4C} for 4C fit from Monte-Carlo and Data, here S represents the signal and $S+B$ represents signal plus background. For Λ and $\overline{\Lambda}$ candidates selection, a mass constraint of $5MeV/c^2$ and $\chi^2_{4C} < 100$ are chosen, by optimizing $\frac{S}{\sqrt{S+B}}$ as shown in Figure 4.13.

4.5 Background Study

After final event selection for the invariant mass distributions, we investigate the possible background events that may affect our expected signal region. We study the possible background events using 106M $\psi(2S)$ Inclusive MC samples and as well 100 thousand MC sample for each decay channel with the same final states mentioned in PDG(2010). The background events from inclusive Monte-Carlo topology analysis are listed in the Table. 4.1

Table 4.1: MC topology

No.	Decay chain	final States	N_{Evt}
1	$\psi(2S) \to \overline{\Lambda}\Sigma^{*-}\pi^+$ $\overline{\Lambda} \to \overline{p}\pi^+$, $\Sigma^{*-} \to \Lambda\pi^-$,$\Lambda \to p\pi^-$	$p\overline{p}\pi^+\pi^+\pi^-\pi^-$	226
2	$\psi(2S) \to \overline{\Sigma}^{*+}\Lambda\pi^-$ $\Lambda \to p\pi^-$, $\Sigma^{*+} \to \overline{\Lambda}\pi^+$,$\overline{\Lambda} \to \overline{p}\pi^+$	$p\overline{p}\pi^+\pi^+\pi^-\pi^-$	229
3	$\psi(2S) \to \overline{\Lambda}\rho^0\Lambda$ $\overline{\Lambda} \to \overline{p}\pi^+$, $\rho^0 \to \pi^+\pi^-$,$\Lambda \to p\pi^-$	$p\overline{p}\pi^+\pi^+\pi^-\pi^-$,	89
4	$\psi(2S) \to J/\psi\pi^+\pi^-$, $J/\psi \to \overline{\Lambda}\Lambda$, $\overline{\Lambda} \to \overline{p}\pi^+$, $\Lambda \to \overline{p}\pi^+$	$p\overline{p}\pi^+\pi^+\pi^-\pi^-$,	56
5	$\psi(2S) \to p\overline{\Lambda}K^{*-}$ $\overline{\Lambda} \to p\pi^-, K^{*-} \to K^0\pi^-, K^0 \to K_S^0$ $K_S^0 \to \pi^+\pi^-$	$p\overline{p}\pi^+\pi^+\pi^-\pi^-$	16
6	$\psi(2S) \to \Lambda\overline{p}K^{*+}$, $\Lambda \to p\pi^-, K^{*+} \to K^0\pi^+, K^0 \to K_S^0$ $K_S^0 \to \pi^+\pi^-$	$p\overline{p}\pi^+\pi^+\pi^-\pi^-$	16
7	$\psi(2S) \to \omega\Lambda\overline{\Lambda}$, $\omega \to \pi^-\pi^+, \Lambda \to p\pi^-, \overline{\Lambda} \to \overline{p}\pi^+$ $K_S^0 \to \pi^+\pi^-$	$p\overline{p}\pi^+\pi^+\pi^-\pi^-$	11
8	$\psi(2S) \to \overline{\Sigma}^{*+}\Sigma^{*-}, \overline{\Sigma}^{*+} \to \overline{\Lambda}\pi^+$, $\Sigma^{*-} \to \Lambda\pi^-, \Lambda \to p\pi^-, \overline{\Lambda} \to \overline{p}\pi^+$ $K_S^0 \to \pi^+\pi^-$	$p\overline{p}\pi^+\pi^+\pi^-\pi^-$	5
9	$\psi(2S) \to \pi^+\pi^- J/\psi$ $J/\psi \to \overline{p}\pi^-\overline{p}\pi^+$	$p\overline{p}\pi^+\pi^+\pi^-\pi^-$	3
10	$\psi(2S) \to \pi^+\pi^- J/\psi$ $J/\psi \to \Delta^{++}\overline{p}\pi^-, \Delta^{++} \to p\pi^+$	$p\overline{p}\pi^+\pi^+\pi^-\pi^-$	3

4.6 Detection Efficiency

The Monte-Carlo sample is used to estimate the the detection efficiency. The number of Λ events are obtained after applying the final event selection and all the mass constraints. The invariant mass distributions of $p\pi^-$ and $\overline{p}\pi^+$ are shown in the Fig. 4.10 and 4.11. The number of events selected for Λ and $\overline{\Lambda}$ are $N_\Lambda = 6548 \pm 81$ and $N_{\overline{\Lambda}} = 6546 \pm 81$. So the average number of observed events are $N_{obs} = 6547 \pm 81$. The efficiency is calculated using the formula

$$\varepsilon = \frac{N_{obs}}{N_{generated}} \times 100\%$$

where $N_{generated} = 100000$. Thus the detection efficiency is determined to be 6.55%

4.7 Fit Results

Based on the above event selection criteria and mass cuts listed above, the events for the decay process $\psi(2S) \to \Lambda\overline{\Lambda}\pi^+\pi^-$ excluding intermediate resonances, are selected. The invariant mass distributions of Λ and $\overline{\Lambda}$ are shown in figure:4.14. The Gaussian function is used to describe signal events and first order Chebychev polynomial for background events. The mass resolution is obtained with Monte-Carlo simulation. The mass resolution for Λ and $\overline{\Lambda}$ is shown in Fig.4.15 and its value is $\sigma = 0.0012 GeV/c^2$.

The number of events observed for Λ and $\overline{\Lambda}$ are $N_\Lambda = 373 \pm 20$ and $N_\Lambda = 390 \pm 21$ respectively. The average number of signal events using the unconstrained averaging method are $N_{obs} = 381 \pm 14$.

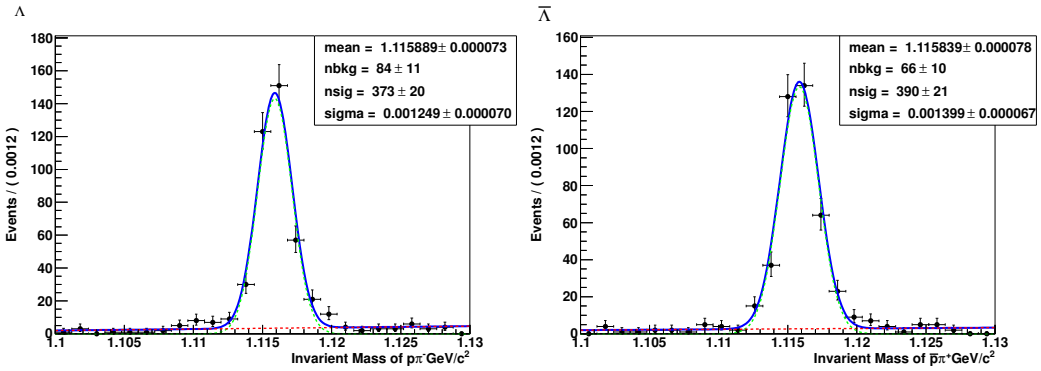

Figure 4.14: Invariant mass distribution of Λ (left) and $\overline{\Lambda}$ (right). The signal is fitted with Gaussian function (green line) and Chebchev polynomial (red dashed line) is used to for signal events and background events respectively.

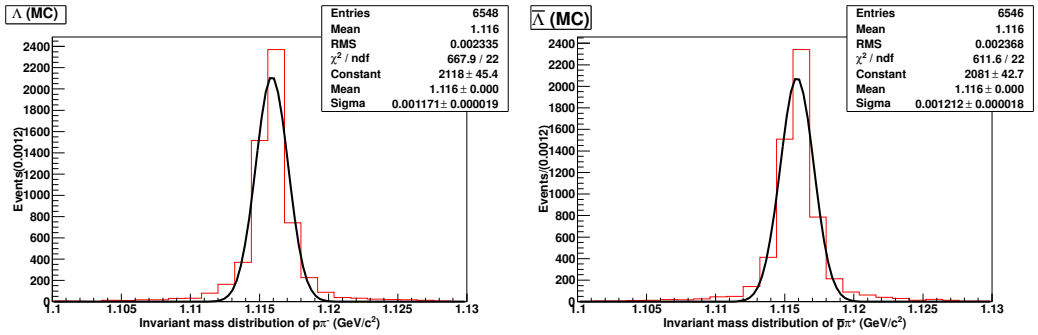

Figure 4.15: Invariant mass distribution of Λ (left) and $\overline{\Lambda}$ (right). The Monte-Carlo signal is fitted with Gaussian function for mass resoultion.

4.8 Determination of Branching Fraction

The branching fraction $\mathcal{B}$ of the decay process $\psi(2S) \to \Lambda\overline{\Lambda}\pi^+\pi^-$ excluding intermediate resonances, is determined using the formula

$$\mathcal{B}(\psi(2S) \to \Lambda\overline{\Lambda}\pi^+\pi^-) = \frac{N_{obs}}{N_{\psi(2S)} \times \varepsilon_{MC} \times (\mathcal{B}_{(\Lambda\to p\pi)})^2}$$

Here

$$\mathcal{B}_{(\Lambda\to p\pi)} = (63.9 \pm 0.5)\% = (63.9 \pm 0.5) \times 10^{-2}$$

Both above values are taken from PDG 2010 and $N_{\psi(2S)} = 106M$ REFERENCE. The MC efficiency is $\varepsilon_{MC} = (6.55 \pm 0.08)\%$. By substituting all these value, we get

$$\mathcal{B}(\psi(2S) \to \Lambda\overline{\Lambda}\pi^+\pi^-) = (1.34 \pm 0.05) \times 10^{-4}$$

The error is statistical only. Now after including systematic errors, given in Table. 4.2, the branching fraction estimated to be

$$\mathcal{B}(\psi(2S) \to \Lambda\overline{\Lambda}\pi^+\pi^-) = (1.34 \pm 0.05_{stat} \pm 0.24_{sys}) \times 10^{-4}$$

4.9 Intermediate Resonances

The decay process $\psi(2S) \to \Lambda\overline{\Lambda}\pi^+\pi^-$ has some intermediate states. The invariant mass distributions of $\pi^-\Lambda$, $\pi^+\overline{\Lambda}$, $\pi^+\Lambda$ and $\pi^-\overline{\Lambda}$ as shown in Figures 4.7 and 4.8, which clearly indicate the existence of Ξ^-, $\overline{\Xi}^+$, Σ^{*-}, $\overline{\Sigma}^{*+}$, Σ^{*+} and $\overline{\Sigma}^{*-}$ signals. These figures show that there are intermediate resonances i.e. $\psi(2S) \to \Sigma^{*+}\overline{\Sigma}^{*-}$, $\psi(2S) \to \Xi^-\overline{\Xi}^+$ etc.

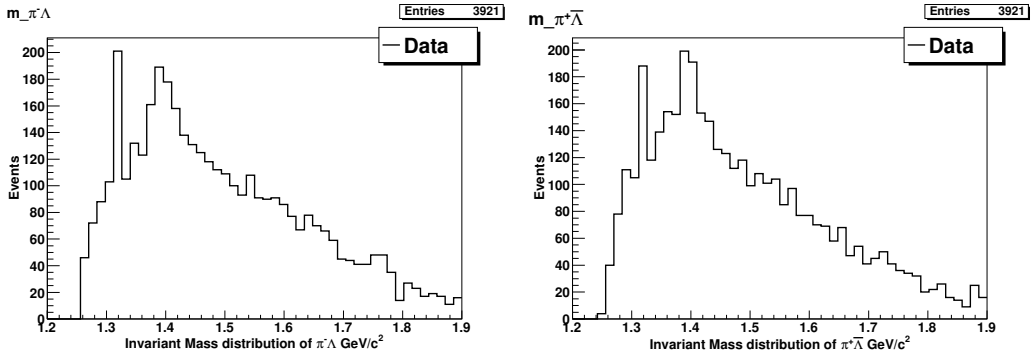

Figure 4.16: Invariant mass distribution of $\pi^-\Lambda$ (left) and $\pi^+\overline{\Lambda}$(right).

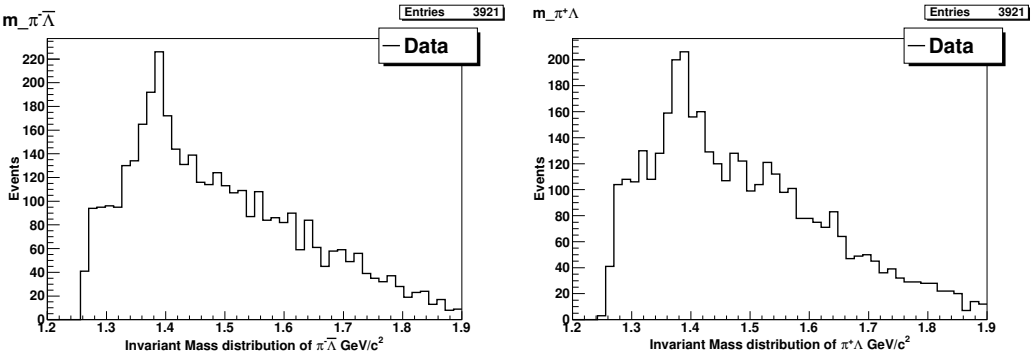

Figure 4.17: Invariant mass distribution of $\pi^-\overline{\Lambda}$ (left) and $\pi^+\Lambda$ (right).

4.10 Analysis of $\psi(2S) \to \Sigma^{*+}\overline{\Sigma}^{*-}$

The decay chain of this process is $\psi(2S) \to \Sigma^{*+}\overline{\Sigma}^{*-}$ where $\Sigma^{*+} \to \pi^+\Lambda$, $\Lambda \to p\pi^-$ and $\overline{\Sigma}^{*-} \to \pi^-\overline{\Lambda}$, $\overline{\Lambda} \to \bar{p}\pi^+$. There are six charged tracks in the final state i.e. one proton, one anti-proton, two π^+ and two π^-. To perform the analysis, we have generated 100 thousand Monte-Carlo sample for the decay process, using J2BB2 generator. Since there are also six charge tracks in the final state, therefore candidate events are selected according to selection criteria mentioned in section 4.3. At first, we have reconstructed Λ and $\overline{\Lambda}$ candidates by applying vertex fits, thereby selecting the right π^+ and π^- which are coming from Σ^{*+} and $\overline{\Sigma}^{*-}$. After applying vertex fit, we reconstruct Σ^{*+} and $\overline{\Sigma}^{*-}$ candidates by imposing 4C kinematic fitting from the combination of $\Lambda\pi^+$ and $\overline{\Lambda}\pi^-$. The events with $\chi^2_{4C} < 100$ are selected for final events selection. For invariant mass distribution plots of $\Lambda\pi^+$ and $\overline{\Lambda}\pi^-$, we used following mass constraints:

- $\mid M_{p\pi^-} - M_{\Lambda} \mid < 0.005 GeV/c^2$
- $\mid M_{\bar{p}\pi^+} - M_{\overline{\Lambda}} \mid < 0.005 GeV/c^2$
- $\mid M_{(\pi^-\Lambda)} - M_{\Xi^-} \mid > 0.013 GeV/c^2$
- $\mid M_{(\pi^+\overline{\Lambda})} - M_{\Xi^+} \mid > 0.013 GeV/c^2$
- $\mid M_{(\pi^+\Lambda)} - M_{\Sigma^{*+}} \mid < 0.09 GeV/c^2$ for $\overline{\Sigma}^{*-}$
- $\mid M_{(\pi^-\overline{\Lambda})} - M_{\overline{\Sigma}^{*-}} \mid < 0.09 GeV/c^2$ for Σ^{*+}
- $\mid M_{(\Lambda\overline{\Lambda})} - M_{J/\psi} \mid > 0.008 GeV/c^2$

- $\mid DecayLength_{\Lambda} \mid > 0.005m$
- $\mid DecayLength_{\overline{\Lambda}} \mid > 0.005m$

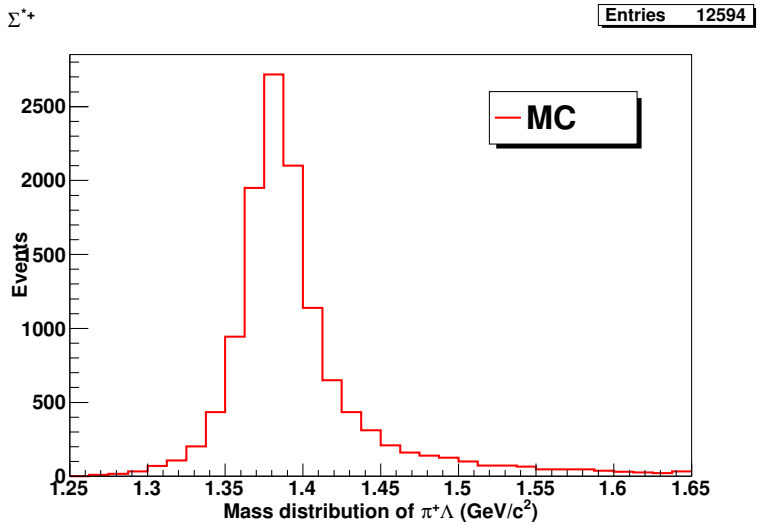

Figure 4.18: Invariant mass distribution of $\Lambda\pi^{+}$.

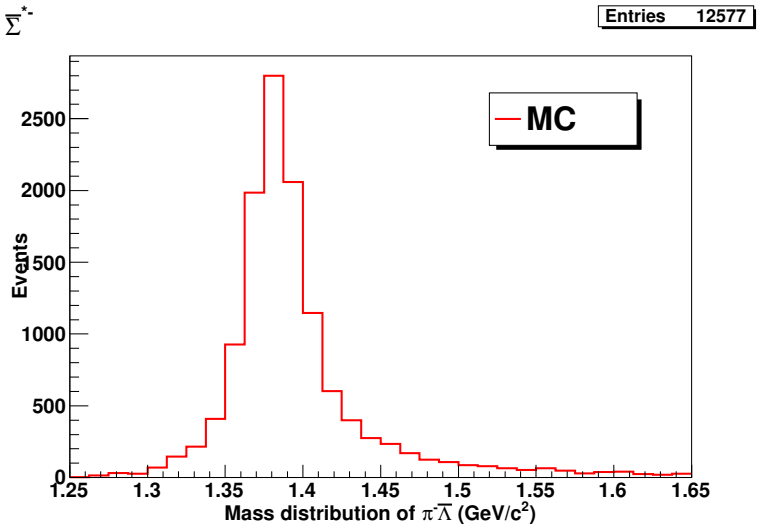

Figure 4.19: Invariant mass distribution of $\overline{\Lambda}\pi^{-}$.

The mass resolutions are determined with single Gaussian fit to Monte-Carlo.

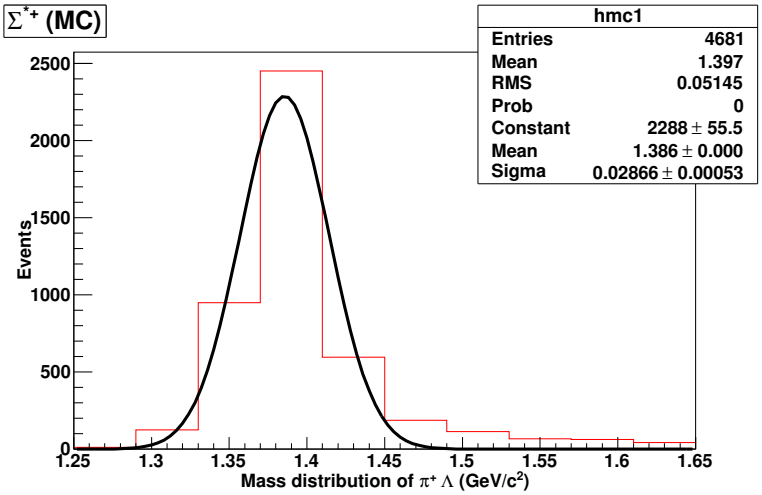

Figure 4.20: Invariant mass distribution of $\Lambda\pi^+$.

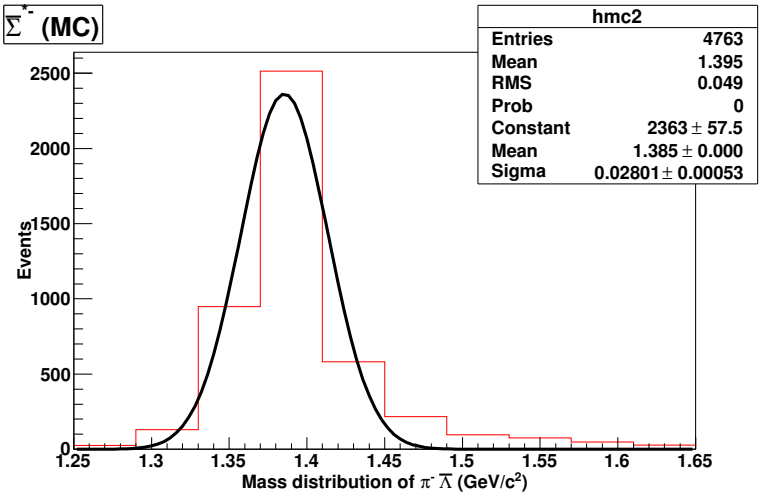

Figure 4.21: Invariant mass distribution of $\overline{\Lambda}\pi^-$.

4.10.1 Fit Results

After final event selection,the Invariant mass distributions of $\Lambda\pi^+$ and $\overline{\Lambda}\pi^-$ are fitted with Gaussian function and third order ChebyChev background polynomial. The blue line represents the model fitting to data points, green line represents the Gaussian fitting and red dashed line shows the third order Chebychev background polynomial. The Figures 4.22 and 4.23 show the fit results.

4.10.2 Determination of Branching Fraction

The branching fraction $\mathcal{B}$ can be determined using the formula

$$\mathcal{B}(\psi(2S) \to \Sigma^{*+}\overline{\Sigma}^{*-}) = \frac{N_{obs}}{N_{\psi(2S)} \times \varepsilon_{MC} \times (\mathcal{B}_{(\Sigma\to\Lambda\pi)})^2(\mathcal{B}_{(\Lambda\to p\pi)})^2}$$

Here

$$\mathcal{B}_{(\Sigma\to\Lambda\pi)} = (87.0 \pm 1.5)\% = (87.0 \pm 1.5) \times 10^{-2}$$

and

$$\mathcal{B}_{(\Lambda\to p\pi)} = (63.9 \pm 0.5)\% = (63.9 \pm 0.5) \times 10^{-2}$$

The branching fraction of intermediate state are taken from [21] and total number of $\psi(2S)$ is $N_{\psi(2S)} = 106M$ [72].

From fit results, the number of observed events are $N_{obs} = 154 \pm 22$ for Σ^{*+} and $N_{obs} = 130 \pm 18$ for $\overline{\Sigma}^{*-}$, So the average number of signal events is 140 ± 14. By Substituting all these values, we get

$$\mathcal{B}(\psi(2S) \to \Sigma^{*+}\overline{\Sigma}^{*-}) = (3.39 \pm 0.34) \times 10^{-5}$$

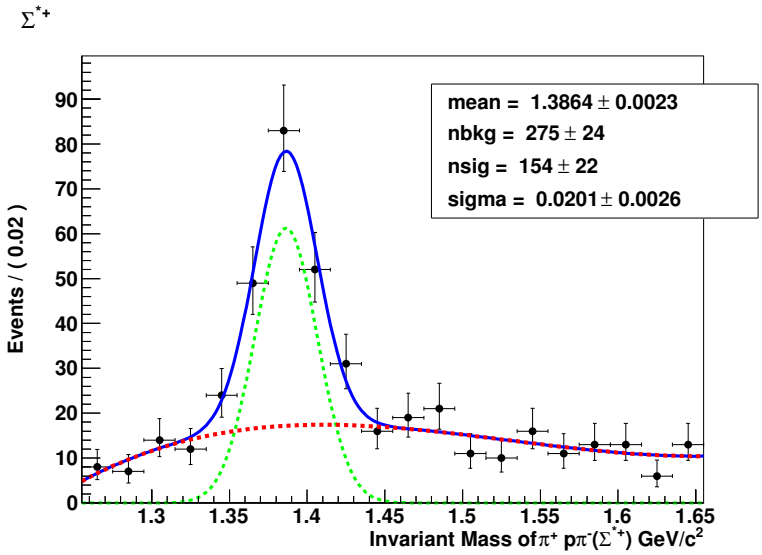

Figure 4.22: Invariant mass distribution of $\Lambda\pi^+$.

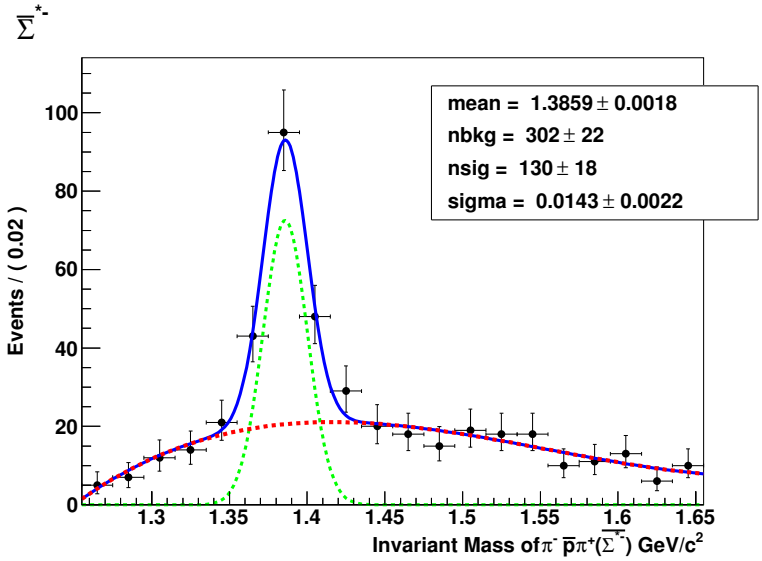

Figure 4.23: Invariant mass distribution of $\overline{\Lambda}\pi^-$.

Here error is statistical one. By including systematic errors, given in Table.4.3, the branching fraction is determined to be

$$\mathcal{B}(\psi(2S) \to \Sigma^{*+}\overline{\Sigma}^{*-}) = (3.39 \pm 0.34_{stat} \pm 0.61_{sys}) \times 10^{-5}$$

4.11 Analysis of $\psi(2S) \to \Xi^-\overline{\Xi}^+$

To study the intermediate resonances of Ξ^- and $\overline{\Xi}^+$, we have generated 100 thousand Monte-Carlo sample of the decay process $\psi(2S) \to \Xi^-\overline{\Xi}^+$ using PHSP generator. In this decay process $\psi(2S) \to \Xi^-\overline{\Xi}^+$ followed by $\Xi^- \to \Lambda\pi^-$ and $\overline{\Xi}^+ \to \overline{\Lambda}\pi^+$ and $\Lambda \to p\pi^-$ and $\overline{\Lambda} \to \overline{p}\pi^+$

4.11.1 Event Selection

This decay process involves six charged tracks in the final state, so initial selection criteria is same as mentioned in the section 4.3. In order to eliminate the background events, we apply some mass constraints within 3σ. For the invariant mass distribution plots of $\Lambda\pi^+$ and $\overline{\Lambda}\pi^-$, we use the following mass constraints.

- $\mid M_{p\pi^-} - M_{\Lambda} \mid < 0.005 GeV/c^2$
- $\mid M_{\overline{p}\pi^+} - M_{\overline{\Lambda}} \mid < 0.005 GeV/c^2$
- $\mid M_{(\pi^-\Lambda)} - M_{\Xi^-} \mid < 0.013 GeV/c^2$ for $\overline{\Xi}^+$
- $\mid M_{(\pi^+\overline{\Lambda})} - M_{\Xi^+} \mid < 0.013 GeV/c^2$ for Ξ^-
- $\mid M_{(\pi^+\Lambda)} - M_{\Sigma^{*+}} \mid > 0.09 GeV/c^2$
- $\mid M_{(\pi^-\overline{\Lambda})} - M_{\overline{\Sigma}^{*-}} \mid > 0.09 GeV/c^2$
- $\mid M_{(\Lambda\overline{\Lambda})} - M_{J/\psi} \mid > 0.008 GeV/c^2$
- $\mid M_{\eta} - M_{\pi^+\pi^-} \mid > 0.009 GeV/c^2$

- $\mid DecayLength_{\Lambda} \mid > 0.005m$
- $\mid DecayLength_{\overline{\Lambda}} \mid > 0.005m$

The $\Lambda\pi^-$ and $\overline{\Lambda}\pi^+$ candidate events have been selected after 4-C kinematic fitting, candidates with $\chi^2_{4C} < 100$ are selected for final event selection. The invariant mass distributions for Ξ^- and $\overline{\Xi}^+$ are shown in the Figure: 4.25

The number of signal events for Ξ^- and $\overline{\Xi}^+$ from Monte-Carlo after final event selection is given are given $N_{\Xi^-} = 2920 \pm 54$ and $N_{\overline{\Xi}^+} = 2895 \pm 54$, so the average number for $\psi(2S) \to \Xi^-\overline{\Xi}^+$ is $N_{\Xi^-\overline{\Xi}^+} = 2907 \pm 54$. Thus the average efficiency is

$$\varepsilon = 2.91\%$$

4.11.2 Fit Results

After final event selection, the invariant mass distributions of $\Lambda\pi^-$ for Ξ^- and $\overline{\Lambda}\pi^+$ for $\overline{\Xi}^+$ are shown in Figures 4.26 and 4.27. Here the invariant mass distributions are fitted with Gaussian function with first order Chebychev background polynomial. The blue line represents the model fitting to data points, green line shows the Gaussian fitting and red dashed line represents the background polynomial. The number of observed events are $N_{obs} = 41.8 \pm 6.5$ for Ξ^- and $N_{obs} = 42.4 \pm 6.5$ for $\overline{\Xi}^+$, so the average number of observed signal events, using unconstrained method is $N_{obs} = 40 \pm 4$.

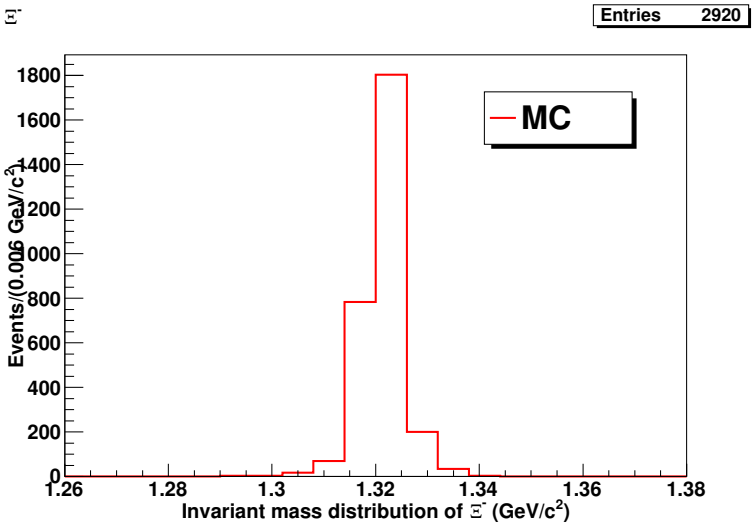

Figure 4.24: Invariant mass distribution of $\Lambda\pi^-$ after final event selection, from $\psi(2S) \to \Xi^-\overline{\Xi}^+$ to determine efficiency.

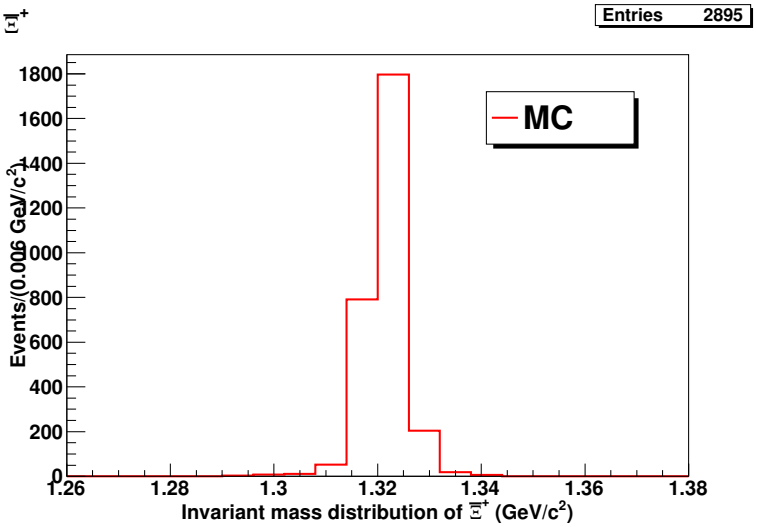

Figure 4.25: Invariant mass distribution of $\overline{\Lambda}\pi^+$ after final event selection, from $\psi(2S) \to \Xi^-\overline{\Xi}^+$ to determine efficiency.

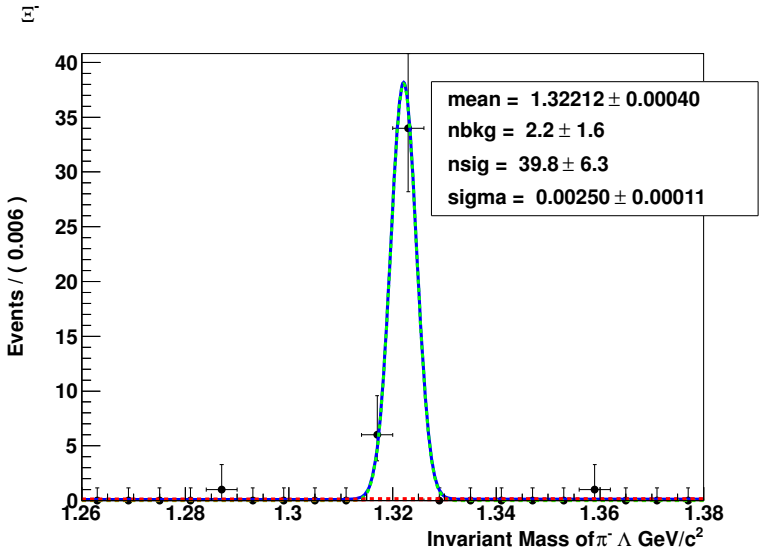

Figure 4.26: Invariant mass distribution of $\Lambda\pi^-$ after final event selection, The blue line represents the model fitting to data points and green line shows the Gaussian fitting and red dashed line represents the background polynomial.

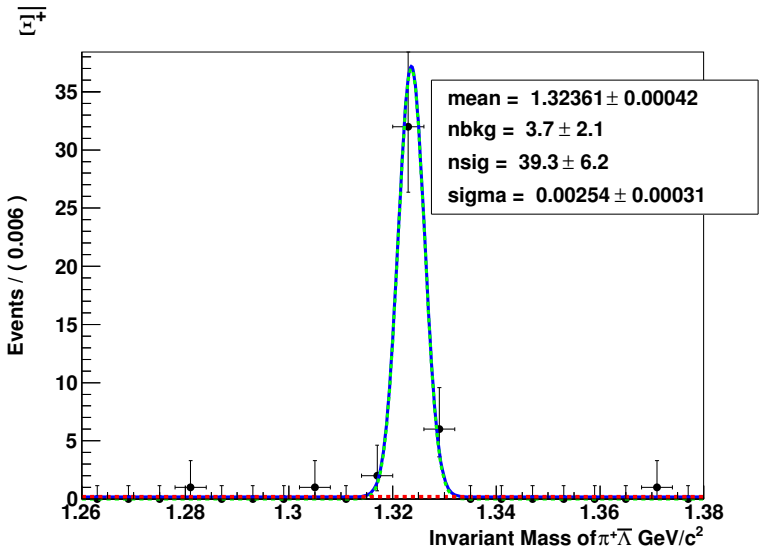

Figure 4.27: Invariant mass distribution of $\overline{\Lambda}\pi^+$.The blue line represents the model fitting to data points and green line shows the Gaussian fitting and red dashed line represents the background polynomial.

4.11.3 Determination of Branching Fraction

The branching fraction $\mathcal{B}$ can be determined using the formula:

$$\mathcal{B}(\psi(2S) \to \Xi^-\overline{\Xi}^+) = \frac{N_{obs}}{N_{\psi(2S)} \times \varepsilon_{MC} \times (\mathcal{B}_{(\Xi\to\Lambda\pi)})^2(\mathcal{B}_{(\Lambda\to p\pi)})^2}$$

Here

$$\mathcal{B}_{(\Xi\to\Lambda\pi)} = (99.887 \pm 0.035)\% = (99.887 \pm 0.035) \times 10^{-2}$$

and

$$\mathcal{B}_{(\Lambda\to p\pi)} = (63.9 \pm 0.5)\% = (63.9 \pm 0.5) \times 10^{-2}$$

. The values of branching fraction for intermediate state are taken from [21] and total number of $\psi(2S)$ is $N_{\psi(2S)} = 106M$ [72]. In order to determine the efficiency ε_{MC}, 100 thousand MC sample of the decay mode $\psi(2S) \to \Xi^-\overline{\Xi}^+$ are generated using J2BB1 generator. using the formula

$$\varepsilon_{MC} = \frac{N_{selected}}{N_{generated}} \times 100\% = (2.90\%$$

So, by substituting all these values, we get

$$\mathcal{B}(\psi(2S) \to \Xi^-\overline{\Xi}^+) = (3.15 \pm 0.35) \times 10^{-5}$$

the error is statistical only.

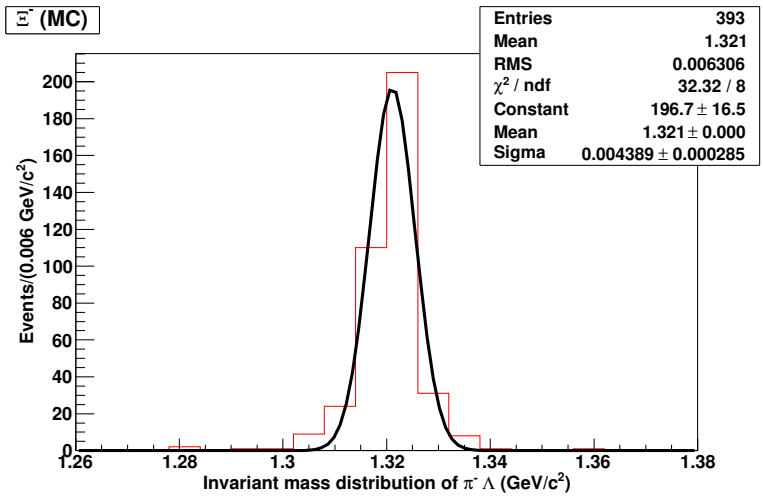

Figure 4.28: Invariant mass distribution of $\Lambda\pi^-$ after final event selection, from $\psi(2S) \to \Xi^-\overline{\Xi}^+$ to determine mass resolution.

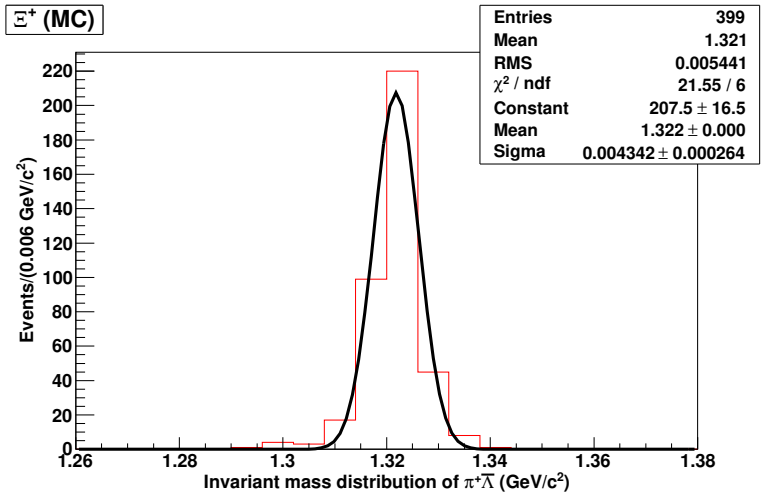

Figure 4.29: Invariant mass distribution of $\overline{\Lambda}\pi^+$ after final event selection, from $\psi(2S) \to \Xi^-\overline{\Xi}^+$ to determine mass resolution.

4.12 Systematic Error Analysis

In this section the systematic error analysis is presented. The systematic errors in our study are mainly arises from total number of $\psi(2S)$ events, charged track detection efficiency, particle identification, vertex fit, 4C kinematic fit and uncertainty of the intermediate resonance branching fraction. We estimate all these errors, but the errors due to vertex and 4C kinematic fits are discussed in detail.

4.12.1 Charged track detection efficiency

The systematic error for charge track detection is found to be 1% per charge track. Since there are six charge tracks in our analysis, the systematic uncertainty dueMDC charge track detection efficiency is taken as is 6%.

4.12.2 Particle identification(PID)

The uncertainty due to particle identification is determined to be 1%. We identify only proton and anti-proton so uncetianty due to particle identification is 2%.

4.12.3 $\Lambda/\overline{\Lambda}$ Reconstruction efficiency

We reconstruct Λ and $\overline{\Lambda}$ by applying primary and secondary vertex fits. So for estimating the Λ and $\overline{\Lambda}$ reconstruction efficieny, we use the decay process $\psi(2S) \rightarrow \Xi^{-}\overline{\Xi}^{+}$. After comparing the relative efficiency of MC and data, we estimate the systematic uncertainty of primary/secondary vertex for Λ is 4%.

4.12.4 4-C kinematic fit

The systematic error from four constraint kinematic fit is performed using by the analysis of the decay process $J/\psi \to \Xi^-\overline{\Xi}^+$ where $\Xi^- \to \Lambda\pi^-$, $\overline{\Xi}^+ \to \overline{\Lambda}\pi^+$, $\Lambda \to p\pi^-$ and $\overline{\Lambda} \to \bar{p}\pi^+$. This decay process also involves six charge tracks in the final state. By comparing the relative efficiencies of Monte-Carlo and data, the systematic error for 4C kinematic fit is estimated as 15.8%. The detailed analysis is described in Appendix A

4.12.5 Branching fraction uncertainties of intermediate resonances

The systematic uncertainty from the branching fraction of intermediate resonances was calculated from the uncertainties in these branching fractions. According to PDG 2010 the branching fraction of Λ, Ξ and Σ are

$$\mathcal{B}(\Lambda \to p\pi^-) = (63.9 \pm 0.5)\%$$

$$\mathcal{B}(\Sigma \to \Lambda\pi) = (87.0 \pm 1.5)\%$$

$$\mathcal{B}(\Xi \to \Lambda\pi) = (99.887 \pm 0.035)\%$$

So uncertainty due to $[\mathcal{B}(\Lambda \to p\pi^-)]^2$ is calculated to be 1.56% uncertainties in the branching fraction of $\psi(2S) \to \Lambda\overline{\Lambda}\pi^+\pi^-$.

For the analysis of $\psi(2S) \to \Xi^-\overline{\Xi}^+$, the uncertainty arising from the uncertainties in the branching fractions of $\Xi \to \Lambda\pi$ and $\Lambda \to p\pi$ so the total uncertainty from $[\mathcal{B} = \Xi \to \Lambda\pi]^2$ and $[\mathcal{B}(\Lambda \to p\pi^-)]^2$ is 0.07% and 1.56%

Table 4.2: Systematic uncertainties for $\psi(2S) \to \Lambda\overline{\Lambda}\pi^+\pi^-$

Source of uncertainty	Uncertainty%
Charge track detection efficiency	6
Particle identification	2
Vertx fit	4
4-C kinematic fit	15.8
Intermediate resonance branching fraction	1.56
Total number of $\psi(2S)$	0.81
	Total = 17.57

Table 4.3: Systematic uncertainties for $\psi(2S) \to \Sigma^{*+}\overline{\Sigma}^{*-}$

Source of uncertainty	Uncertainty%
Charge track detection efficiency	6
Particle identification	2
Vertx fit	4
4-C kinematic fit	15.8
Intermediate resonance branching fraction	3.76
Total number of $\psi(2S)$	0.81
	Total = 17.90

respectively. so the combined effect is evaluated to be 1.6%

For the analysis of $\psi(2S) \to \Sigma^{*+}\overline{\Sigma}^{*-}$, the uncertainties from $[\mathcal{B} = \Sigma \to \Lambda\pi]^2$ and $[\mathcal{B}(\Lambda \to p\pi^-)]^2$ are 3.4% and 1.56% respectively. The combined effect is computed to be 3.76%.

4.12.6 Total number of $\psi(2S)$ data events

The branching fraction for these decay channel is estimated using 106×10^6 data events. The total number of $\psi(2S)$ determined by counting the inclusive hadronic events are $106.41 \times (1.00 \pm 0.81) \times 10^6$ as desribed in [72]. So 0.81% is taken as the source systematic uncertainty in the total number of $\psi(2S)$ data events.

Table 4.4: Systematic uncertainties for $\psi(2S) \to \Xi^-\overline{\Xi}^+$

Source of uncertainty	Uncertainty%
Charge track detection efficiency	6
Particle identification	2
Vertx fit	4
4-C kinematic fit	15.8
Intermediate resonance branching fraction	1.60
Total number of $\psi(2S)$	0.81
	Total = 17.57

Chapter 5

Summary and Conclusion

The basic concepts of Standard Model of Particle Physics, charmonium spectroscopy and BESIII experimental setup have been reviewed. The main highlights of the analysis are as:

- Monte-Carlo simulation of the signal and background decay channels was carried out using PHSP and J2BB2 generator.
- The detection efficiencies and mass resolutions for the signal decay channels and in some cases for background channels, were determined by fitting the relevant invariant mass distributions with single Gaussian function.
- The background analysis was carried out by using $106M$ $\psi(2S)$ Inclusive Monte-Carlo sample.
- Fit results were used to determine the branching fractions of the decay channels to be

$\psi(2S) \to \Lambda\overline{\Lambda}\pi^+\pi^- = (1.34 \pm 0.05_{stat} \pm 0.24_{sys}) \times 10^{-4}$

$\psi(2S) \to \Sigma^{*+}\overline{\Sigma}^{*-} = (3.39 \pm 0.34_{stat} \pm 0.61_{sys}) \times 10^{-5}$

$\psi(2S) \to \Xi^-\overline{\Xi}^+ = (3.15 \pm 0.35_{stat} \pm 0.55_{sys}) \times 10^{-5}$

We can conclude this work as:

- Our results are extremely precise as compared to previously measured branching fractions as is clear from the Table.5.1

Table 5.1: The branching fraction of the decay processes and comparison between our results and PDG valus

decay channel	Our Measurement	PDG Values
$\psi(2S) \to \Lambda\overline{\Lambda}\pi^+\pi^-$	$(1.34 \pm 0.05_{stat} \pm 0.24_{sys}) \times 10^{-4}$	$(2.8 \pm 0.5) \times 10^{-4}$
$\psi(2S) \to \Sigma^{*+}\overline{\Sigma}^{*-}$	$(3.39 \pm 0.34_{stat} \pm 0.61_{sys}) \times 10^{-5}$	$(11 \pm 4) \times 10^{-5}$
$\psi(2S) \to \Xi^-\overline{\Xi}^+$	$(3.15 \pm 0.35_{stat} \pm 0.55_{sys}) \times 10^{-5}$	$(18 \pm 6) \times 10^{-5}$

Appendix A

Systematic Error Analysis for 4C Kinematic fit

To estimate the systematic error for 4C kinematic fit, we use the decay process $J/\psi \to \Xi^-\overline{\Xi}^+$, where $\Xi^- \to \Lambda\pi^-$, $\Lambda \to p\pi^-$ and $\overline{\Xi}^+ \to \overline{\Lambda}\pi^+$, $\overline{\Lambda} \to \overline{p}\pi^+$. We have generated 100,000 Monte-Carlo sample of this decay channel using PHSP generator. There are six charged tracks in the final state, so we use the initial event selection criteria described in the section (4.3). For the selection of candidate events, the all charge tracks are required to pass through vertex fit, after that 4C kinematic fit is performed. The $\Lambda/\overline{\Lambda}$ candidate are selected by comparing the least mass difference, thereby selecting the right π^+ and π^-. Finally Ξ^- and $\overline{\Xi}^+$ candidate are selected by the combination of $\Lambda\pi^-$ and $\overline{\Lambda}\pi^+$ respectively. The invariant mass distributions of $\Lambda\pi^-$ and $\overline{\Lambda}\pi^+$ are obtained after applying the following mass constraints:

- $\mid M_{p\pi^-} - M_\Lambda \mid < 0.005 GeV/c^2$

- $\mid M_{\overline{p}\pi^+} - M_{\overline{\Lambda}} \mid < 0.005 GeV/c^2$
- $\mid M_{(\pi^-\Lambda)} - M_{\Xi^-} \mid < 0.013 GeV/c^2$ for $\overline{\Xi}^+$
- $\mid M_{(\pi^+\overline{\Lambda})} - M_{\Xi^+} \mid < 0.013 GeV/c^2$ for Ξ^-
- $\mid M_{(\pi^+\Lambda)} - M_{\Sigma^{*+}} \mid > 0.09 GeV/c^2$
- $\mid M_{(\pi^-\overline{\Lambda})} - M_{\overline{\Sigma}^{*-}} \mid > 0.09 GeV/c^2$
- $\mid M_{(\Lambda\overline{\Lambda})} - M_{J/\psi} \mid > 0.008 GeV/c^2$
- $\mid M_{\pi^+\pi^-} - M_{\eta} \mid > 0.009 GeV/c^2$

The systematic error is estimated by comparing the relative efficiencies of Monte-Carlo and data by imposing the condition of 4C kinematic fit and without kinematic fit. The efficiency of 4C kinematic fit is defined as

$$\varepsilon = \frac{N_{\Xi^-}(With4Cfit)}{N_{\Xi^-}(Without4Cfit)}$$

where $N_{\Xi^-}(With4Cfit)$ and $N_{\Xi^-}(Without4Cfit)$ are the number of Ξ^- events with 4C fit and without 4C fit respectively. The invariant mass distributions of $\Lambda\pi^-$ and $\overline{\Lambda}\pi^+$ with and without 4C kinematic fit from Monte-Carlo (Figures A.1 and A.2) and from data (Figures A.3 and A.4)respectively. The number of signal events are obtained by fitting the signal with Gaussian function and first order Chebychev backgroud polnomial. The relative efficiencies of 4C kinematic fit for MC ($\frac{717\pm94}{740\pm28} \times 100\% = (96.89 \pm 16.09)\%$) and for data are ($\frac{433\pm21}{531\pm24} \times 100\% = (81.54 \pm 7.64)\%$). By comparing the relative efficiencies of MC and DATA, the systematic error due to 4C kinematic fit is estimated to be (15.84)%.

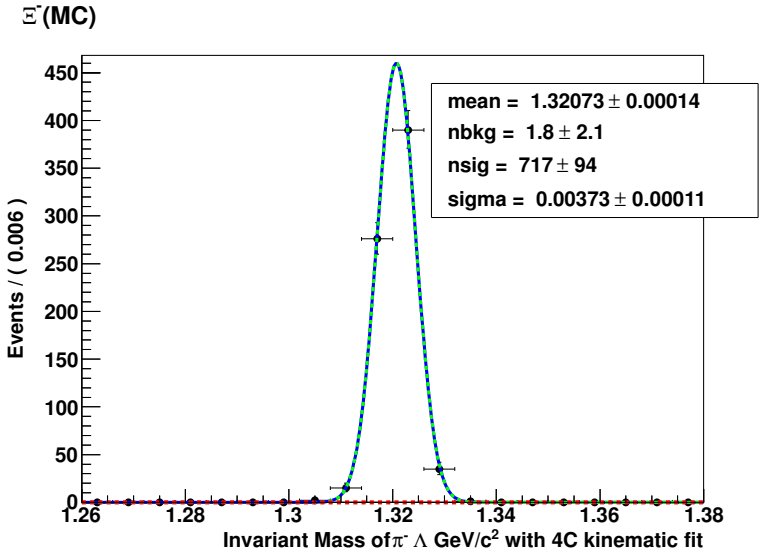

Figure A.1: Invariant mass distribution of $\Lambda\pi^-$ with 4C kinematic fit from Monte-Carlo.

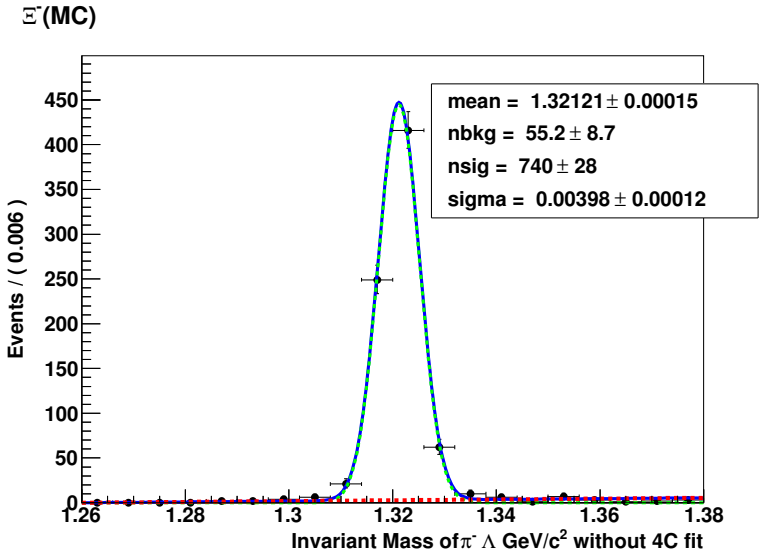

Figure A.2: Invariant mass distribution of $\overline{\Lambda}\pi^+$ with out 4C kinematic fit from Monte-Carlo.

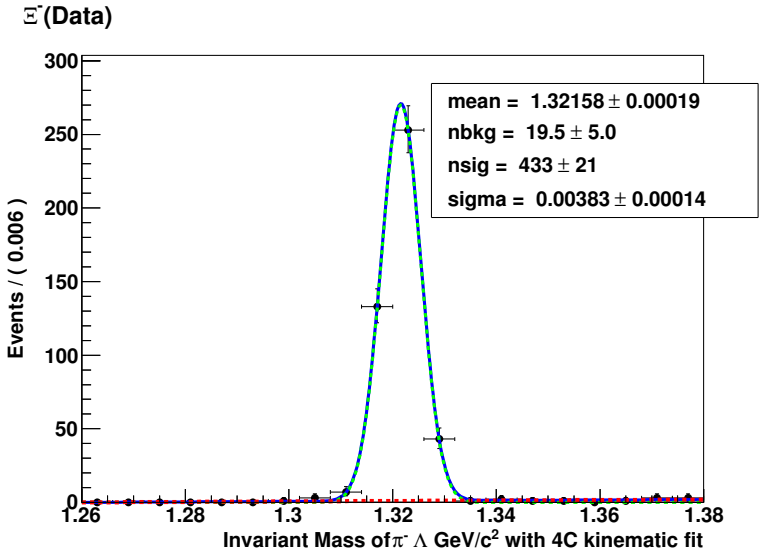

Figure A.3: Invariant mass distribution of $\Lambda\pi^-$ with 4C kinematic fit from Data.

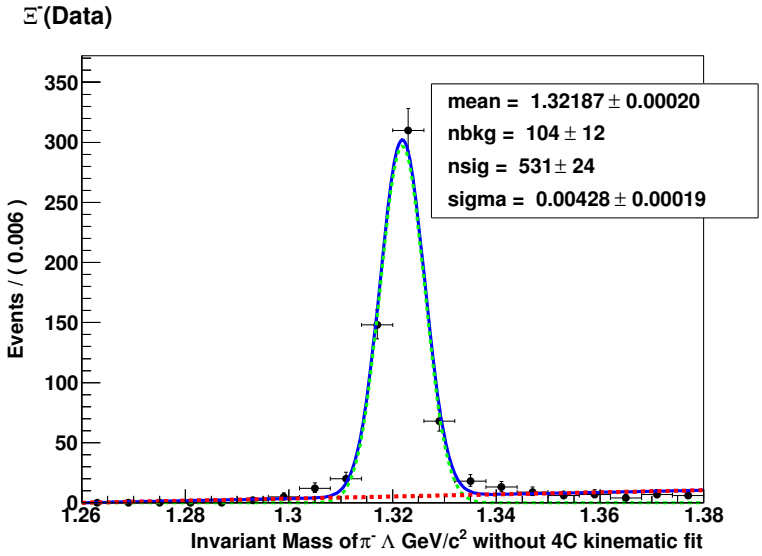

Figure A.4: Invariant mass distribution of $\overline{\Lambda}\pi^+$ with out 4C kinematic fit from Data.

Appendix B

$\Lambda/\overline{\Lambda}$ reconstruction efficiency

In the analysis of $\psi(2S) \to \Lambda\overline{\Lambda}\pi^+\pi^-$, the candidate events of Λ and $\overline{\Lambda}$ have been reconstructed by applying primary and second vertex fit. We select the best candidate event for Λ and $\overline{\Lambda}$ on the basis of least χ^2 values. In order to get pure signal, $\chi^2 < 1000$ and $\chi^2 < 500$ is used for primary and secondary vertex fits respectively. In order to determine the reconstruction efficiency we use the decay process $J/\psi \to \Xi^-\overline{\Xi}^+$, where $\Xi^- \to \Lambda\pi^-$, $\Lambda \to p\pi^-$ and $\overline{\Xi}^+ \to \overline{\Lambda}\pi^+$, $\overline{\Lambda} \to \overline{p}\pi^+$. The vertex fit efficiency is defined as

$$\varepsilon_{1^{st}and2^{nd}vertexfit} = \frac{N_2}{N_1}$$

where N_2 are the events for $p\pi^-$ and $\overline{p}\pi^+$ passing through primary and second verteces and N_1 are the events for $p\pi^-$ and $\overline{p}\pi^+$ reconstructed without primary and secondary verteces. Figures B.1 and B.2 show the statistics of events obtained with and without vertex fit for MC, respectively, and figures B.3 and B.4 shows the same statistics for Data. Here the invariant mass

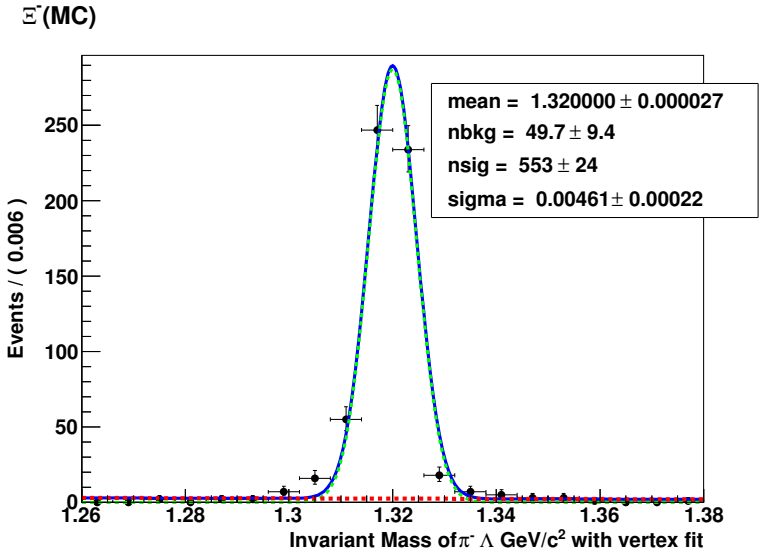

Figure B.1: Invariant mass distribution of $\Lambda\pi^-$ with vertex fit from Monte-Carlo.

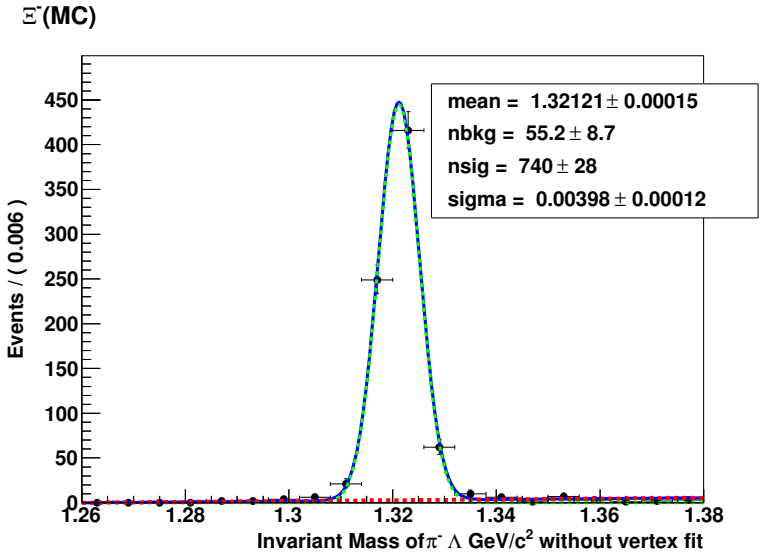

Figure B.2: Invariant mass distribution of $\overline{\Lambda}\pi^+$ without vertex fit from Monte-Carlo.

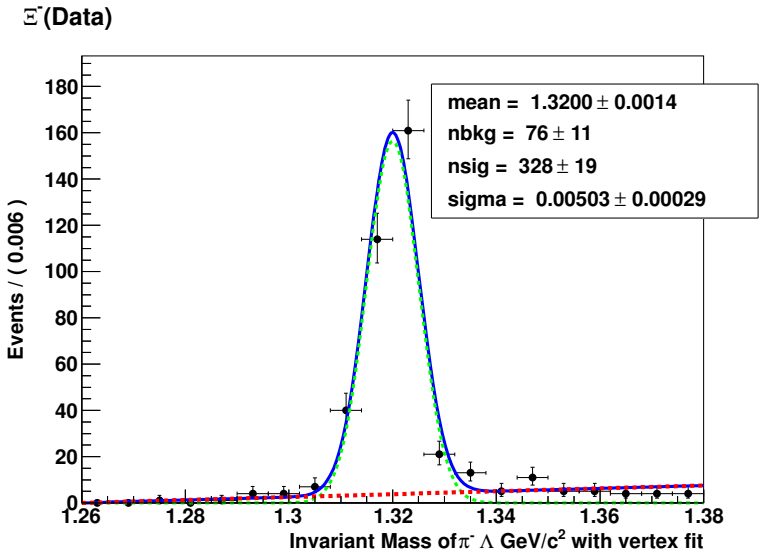

Figure B.3: Invariant mass distribution of $\Lambda\pi^-$ with vertex fit from Data.

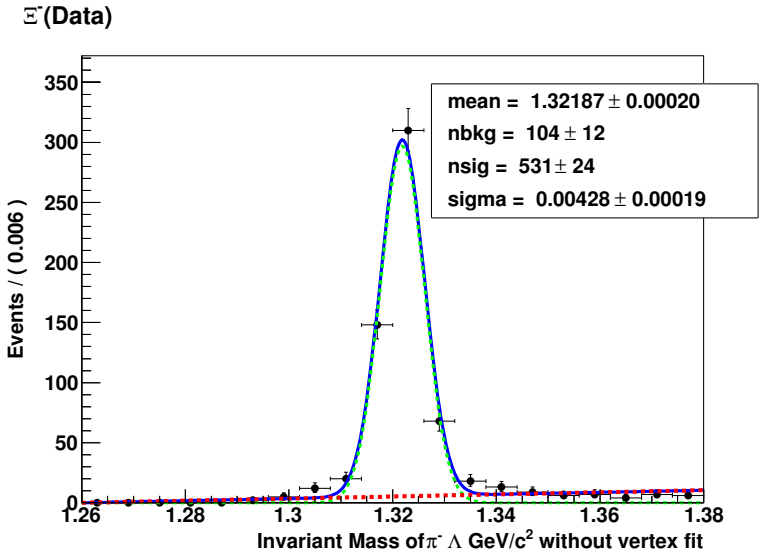

Figure B.4: Invariant mass distribution of $\overline{\Lambda}\pi^+$ without vertex fit from Data.

distributions are fitted with Gaussian function and first order Chebychev background polynaomial for number of signal events. From the statistics shown in the figures, the relative efficiency of vertex fit with primary and secondary vertex for MC signal is

$$\frac{553 \pm 24}{740 \pm 28} \times 100\% = (74.72\pm)\%$$

and the relative efficiency of vertex fit with primary and secondary vertex for Data is

$$\frac{328 \pm 19}{531 \pm 24} \times 100\% = (61.77\pm)\%$$

By comparing the relative efficiency of MC and Data, the systematic error due to primary and secondary vertex fit for Λ and $\overline{\Lambda}$ is 17.33%. So the systematic error for $\Lambda/\overline{\Lambda}$ for primary/secondary vertex fit is estimated to be 4%.

Appendix C

Inclusive Monte-Carlo Background Study

The possible background events that may contribute to the signal region, are studied using 106 M Inclusive Monte-Carlo sample. From this study, it is found that main background is from the decay channels for which invariant mass plots are shown as below:

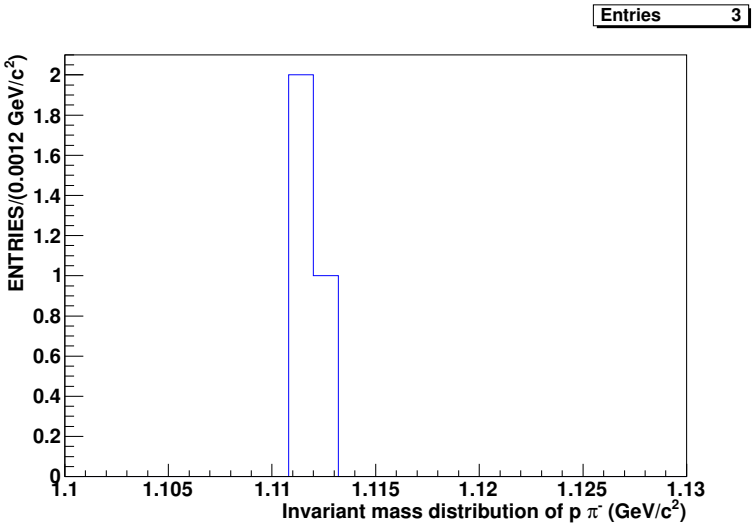

Figure C.1: Invariant mass distribution of $p\pi^-$ from Inclusive MC sample for $\psi(2S) \to \pi^-\pi^+ J/\psi$ where $J/\psi \to \bar{p}\pi^- p\pi^+$.

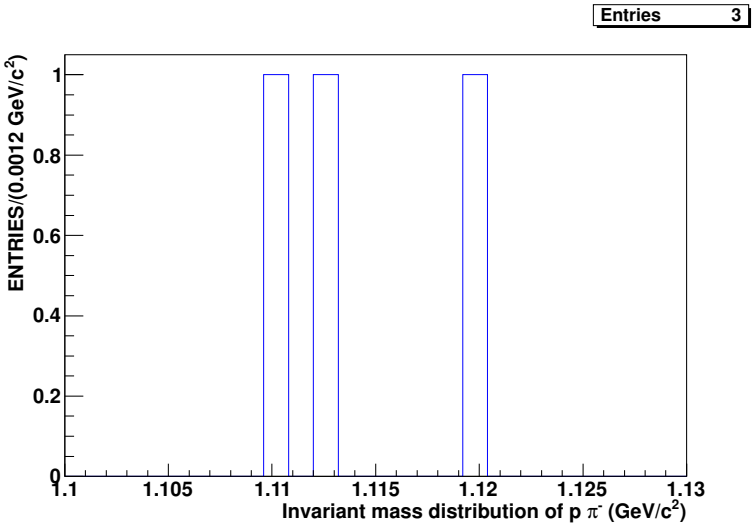

Figure C.2: Invariant mass distribution of $p\pi^-$ from Inclusive MC sample for $\psi(2S) \to \pi^-\pi^+ J/\psi$ where $J/\psi \to \Delta{+}{+}\pi^-\bar{p}$ and $\Delta^{++} \to p\pi^+$.

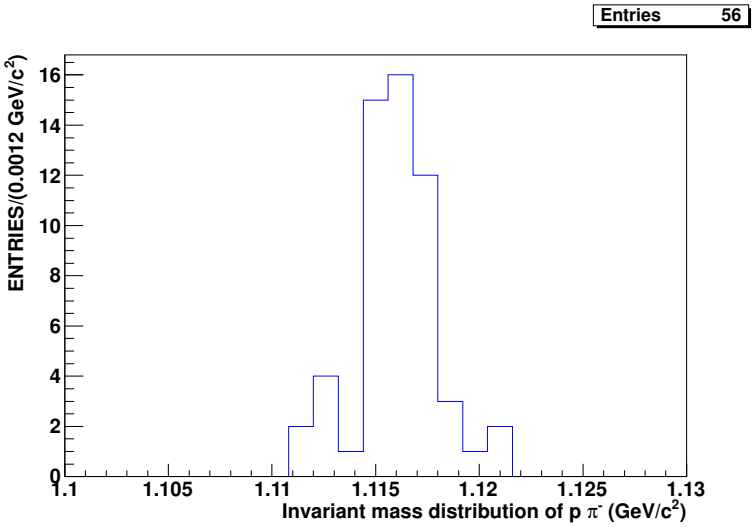

Figure C.3: Invariant mass distribution of $p\pi^-$ from Inclusive MC sample for $\psi(2S) \to J/\psi\pi^+\pi^-$ where $J/\psi \to \Lambda\bar{\Lambda}$ and $\Lambda \to p\pi^-, \bar{\lambda} \to \bar{p}\pi^+$.

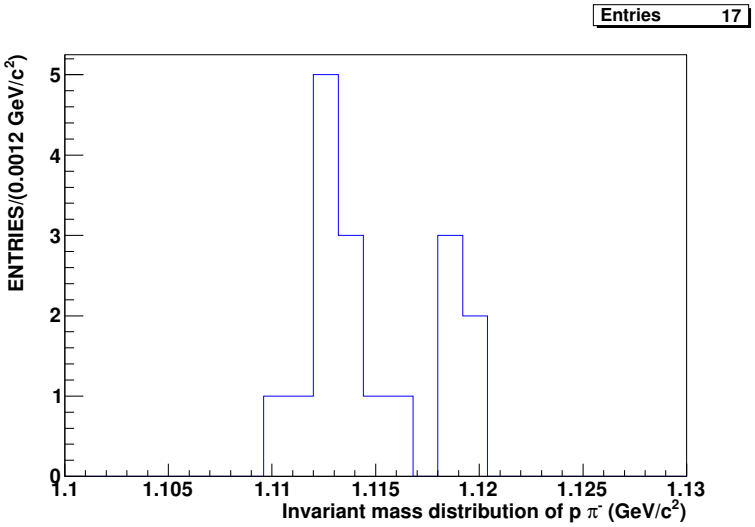

Figure C.4: Invariant mass distribution of $p\pi^-$ from Inclusive MC sample for $\psi(2S) \to p\bar{\Lambda}K^{*-}$ where $\bar{\Lambda} \to \bar{p}\pi^+$ and $K^{*-} \to \bar{K}_o\pi^-, \bar{K}_o \to K_s^o \to \pi^-\pi^+$.

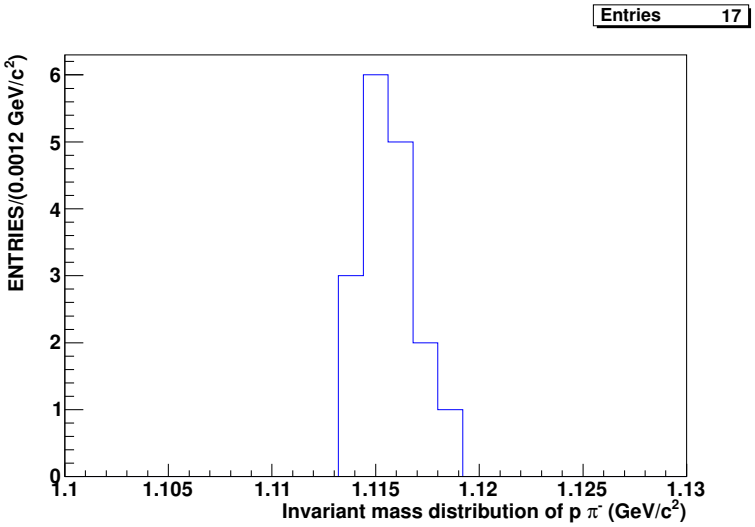

Figure C.5: Invariant mass distribution of $p\pi^-$ from Inclusive MC sample for $\psi(2S) \to \Lambda\bar{p}K^{*+}$ where $\Lambda \to p\pi^-$ and $K^{*+} \to K_o\pi^+, K_o \to K_s^o \to \pi^-\pi^+$.

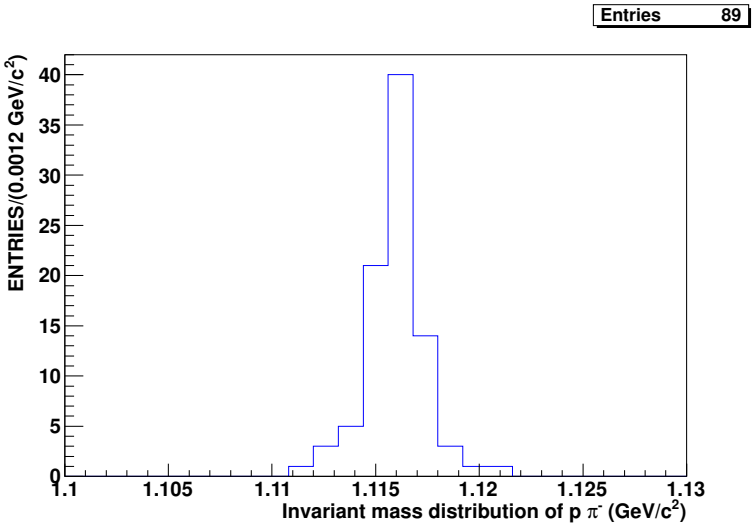

Figure C.6: Invariant mass distribution of $p\pi^-$ from Inclusive MC sample for $\psi(2S) \to \overline{\Lambda}\rho^0\Lambda$, $\overline{\Lambda} \to \overline{p}\pi^+$, $\rho^0 \to \pi^+\pi^-$,$\Lambda \to p\pi^-$.

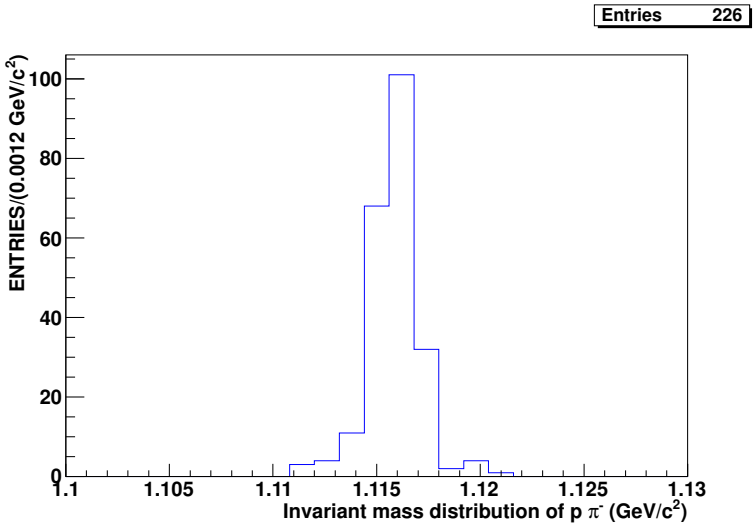

Figure C.7: Invariant mass distribution of $p\pi^-$ from Inclusive MC sample for $\psi(2S) \to \overline{\Lambda}\Sigma^{*-}\pi^+$, $\overline{\Lambda} \to \overline{p}\pi^+$, $\Sigma^{*-} \to \Lambda\pi^-$,$\Lambda \to p\pi^-$.

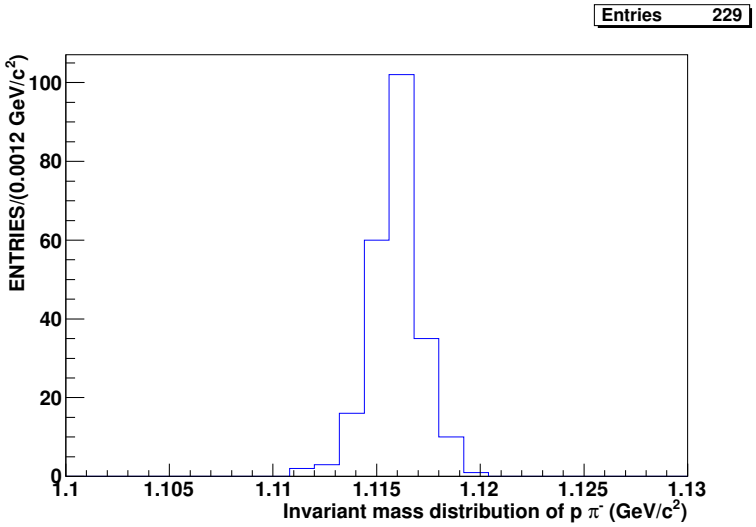

Figure C.8: Invariant mass distribution of $p\pi^-$ from Inclusive MC sample for $\psi(2S) \to \overline{\Sigma}^{*+}\Lambda\pi^-$, $\Lambda \to p\pi^-$, $\Sigma^{*+} \to \overline{\Lambda}\pi^+$,$\overline{\Lambda} \to \overline{p}\pi^+$.

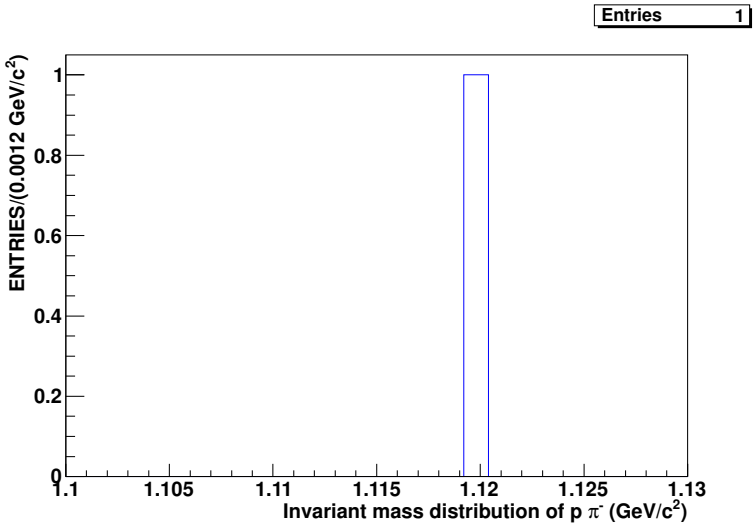

Figure C.9: Invariant mass distribution of $p\pi^-$ from Inclusive MC sample for $\psi(2S) \to \pi^- J/\psi\pi^+$,$J/\psi \to \overline{\Delta}^{++}\overline{p}\pi^+, \overline{\Delta}^{++} \to \overline{p}\pi^-$.

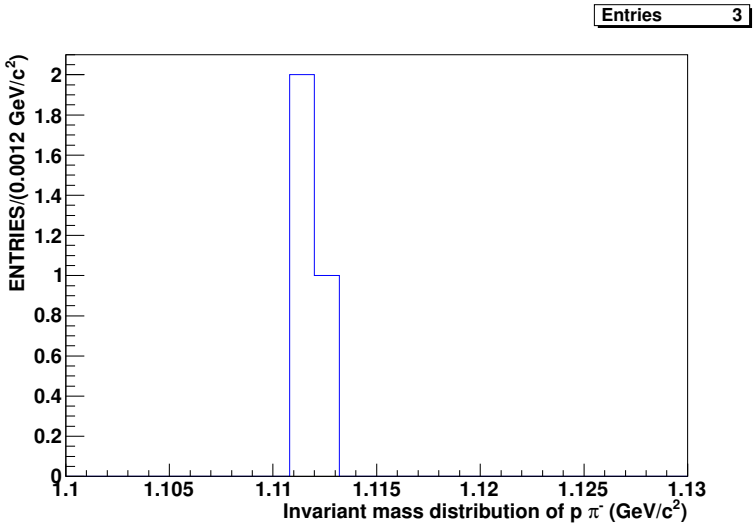

Figure C.10: Invariant mass distribution of $p\pi^-$ from Inclusive MC sample for $\psi(2S) \to \pi^+\pi^- J/\psi$, $J/\psi \to \overline{p}\pi^-\overline{p}\pi^+$.

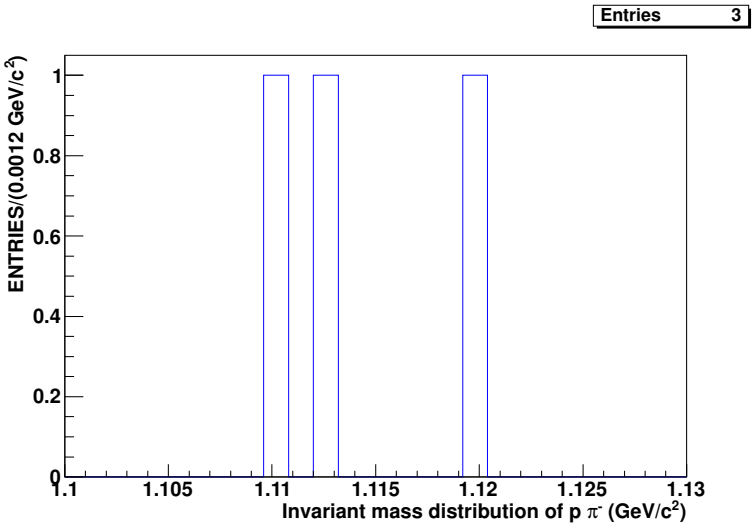

Figure C.11: Invariant mass distribution of $p\pi^-$ from Inclusive MC sample for $\psi(2S) \to \pi^+\pi^- J/\psi$, $J/\psi \to \Delta^{++}\overline{p}\pi^-, \Delta^{++} \to p\pi^+$.

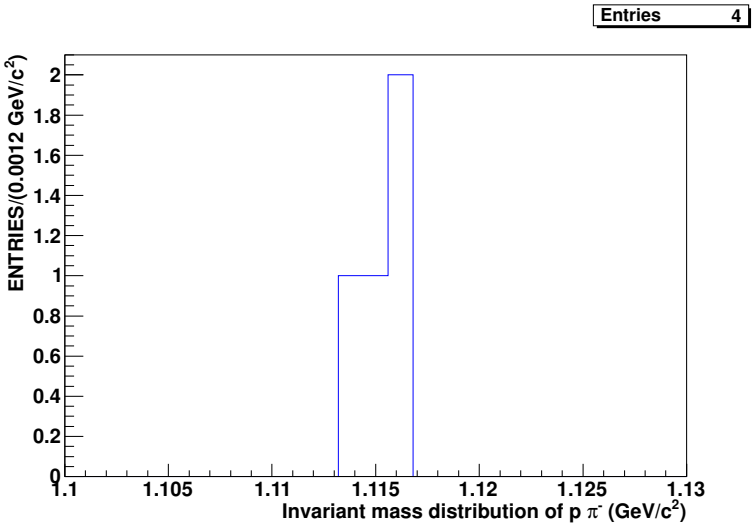

Figure C.12: Invariant mass distribution of $p\pi^-$ from Inclusive MC sample for $\psi(2S) \to \overline{\Sigma}^{*+}\Sigma^{*-}$, $\overline{\Sigma}^{*+} \to \overline{\Lambda}\pi^+$, $\Sigma^{*-} \to \Lambda\pi^-$,$\Lambda \to p\pi^-$, $\overline{\Lambda} \to \overline{p}\pi^+$.

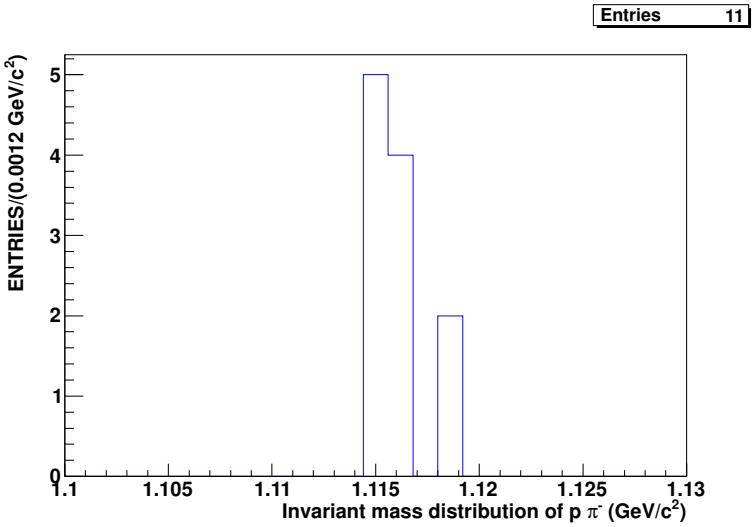

Figure C.13: Invariant mass distribution of $p\pi^-$ from Inclusive MC sample for $\psi(2S) \to \overline{\omega}\Lambda\Lambda$, $\Lambda \to p\pi^-$, $\omega \to \pi^+\pi^-$,$\overline{\Lambda} \to \overline{p}\pi^+$.

Bibliography

[1] Frank Close, Michael Marten, Christine Sutton, *"The Particle odyssey: A journey to the Heart of the Matter"*, Oxfrord University Press, (2002).

[2] M. K. Gaillard, P. D. Grannis, and F. J. Sciulli, *"The Standard Model of Physics"*, Rev. Mod. Phys. **71** (1999) S 96, arXiv: 9812285v1 [hep-ex]

[3] S. Weinberg, *"A Model of Leptons"*, Phy. Rev. Lett. **19** (1967) 1264.

[4] Robert N. Cahn and Gerson Goldhaber, *"The Experimental Foundation of Particle Physics"*, 2nd Edition, Cambridge University Press, 2009.

[5] J. J. Aubert et.al, *"Experimental Observation of a Heavy Particle"*, Phys. Rev. Lett. **33** (1974) 1404.

[6] J. E. Augustin et.al, *"Discovery of Narrow Resonance in e^+e^- Annihilation"*, Phys. Rev. Lett. **33** (1974) 1406.

[7] G. S. Abrams et al., *"Discovery of Second Resonance in e^+e^- Annihilation"*, Phys. Rev. Lett. **33** (1974) 1453.

[8] Jingzhi Zhang, *"Charmonium spectroscopy and decays"*, arXiv:1112.0841v1 [hep-ex].

[9] S. L. Glashow, *"Partial Symmetries of Weak Interactions"*, Nucl. Phys. **22** (1961) 579.

[10] W. N. Cottingham and D. A . Greenwood, *"An Introduction to the Standard model of Particle Physics"*, 2nd Edition, Cambridge University Press, (2007).

[11] A. Das and T. Ferbel, *"Introduction to Nuclear and Particle Physics"*, World Scientific Publishing Co. Pte. Ltd, (2003).

[12] John F. Donoghue, Eugene Golowich and Barry R. Holstein, *"Dynamics of the Standard Model"*, Cambridge University Press (1992).

[13] David Griffith, *"Introduction to Elementary Particles"*, John Wiley and Sons, Inc. (1987).

[14] Murrey. Gell-Mann, 1964, Phys. Lett. **8** (1964) 214.

[15] Bogdan Povh. Klaus Rith. Christoph Scholz. Frank Zetsche, *"Particles and Nuclei: An Introduction to the Physical Concepts"*, 6th Edition, Springer-Verlag Berlin Heidelberg, (2008).

[16] O. W. Greenberg, *"Spin and Unitary-Spin Independence in a Paraquark Model of Baryons and Mesons"*, Phy. Rev. Lett. **13** (1964) 598.

[17] A. Bettini, *"Introduction to Elementary Particle Physics"*, Cambridge University Press, (2008).

[18] Hiroshi Toki, *"Quarks, Baryons and Chiral Symmetry"*, World Scientific Publishing Co. Pte. Ltd, (2001).

[19] Reterived from *"en.wikipedia.org/wiki/Eightfoldway(physics)"* on dated 14 Aug 2012.

[20] V. E. Barnes et al., *"Observation of Hyperon with Strangeness Ninus Three"*, Phys. Rev. Lett. **12** (1964) 204.

[21] Review of Particle Physics, Particle Data Group, *Journal of Physics G*,Vol 37, Number 7A July 2010.

[22] A. W. Hendry and D. B. Lichtenberg, *"The Quark Model"*, Rep. Prog. Phys. **41** (1978).

[23] Roelof Bijker, *"Symmetries in physics"*, arXiv:nucl-th/0509007v1, (2005).

[24] E. L. Hill, *"Hamilton's Principle and the Conservation Theorems of Mathematical Physics"*, Rev. Mod. Phys. **23** (1951) 253.

[25] Colin D. Froggratt and Holger B. Nielson *"Origin of Symmetries"*, World Scientific Publishing Co. Pte. Ltd (1991).

[26] F. Gieres, M. Kibler, C. Lucchesi, O. Piguet, *"Symmetries in Physics"*, Editions Frontier Paris (1997).

[27] E M Henley, *"Parity and Time-Reversal Invariance in Nuclear Physics"*, Annual Review of Nuclear Science, **19** (1969) 365.

[28] Samuel S. M. Wong, *"Introductory Nuclear Physics"*, 2nd Edition, Wiely-VCH Verlag GmbH & Co KGaA (2004).

[29] Donald H. Perkins, *"Introduction to High Energy Physics"* 4th Edition, Cambridge University Press (2000).

[30] D. J. Griffiths, *"Introduction to Quantum Mechanics"*, Prentice Hall, (2005).

[31] C. Bacci et al. *"Preliminary Result of Frascati (ADONE) in the Nature of a new 3.1-GeV Particle Produced in e^+e^- Annihilation"*, Phys. Rev. Lett. **33** (1974) 1408.

[32] W. Braunschweig et al., *"A Measurement of Large Angle e^+e^- Scattering at the 3100 MeV Resonance"*, Phys. Lett. **B 53** (1974) 393.

[33] T. Applequist and H. D. Politzer, *"Heavy Quarks and e^+e Annihilation*, Phys. Rev. Lett. **34** (1975) 43.

[34] T. Applequist and H. D. Politzer, *"Heavy Quarks and Long-lives Hadrons"*, Phys. Rev. Lett. **12**, (1975) 1404 .

[35] T. Applequist, A. De Rujula, H. D. Politzer and S. L. Glashow, *"Spectroscopy of the New Mesons"*, Phys. Rev. Lett. **34** (1975) 365.

[36] E. Eichten, K. Gottfried, T. Kinoshita, J. Kogut, K. D. Lane and T. -M. Yan *"Spectrum of Charmed Quark-Antiquark Bound States"*, Phys. Rev. Lett. **34** (1975) 369.

[37] A. De Rujula and S. L. Glashow, *"Is Bound Charm Found?*, Phys. Rev. Lett. **34** (1975) 46.

[38] C. G. Gallan, R. L. Kingsley, S. B. Treiman, F. W. Wilczek and A. Zee, *"Remarks on the New Resonances at 3.1 and 3.7 GeV"*,Phys. Rev. Lett. **34** (1975) 52.

[39] B. J. Harrington, S. Y. Park, and A. Yildiz, *"Spectrum of Heavy Mesons in e^+e^- Annihilation"*, Phys. Rev. Lett. **34** (1975) 168.

[40] B. J. Harrington, S. Y. Park, and A. Yildiz, *"Orbital Excitation in Charmonium"*, Phys. Rev. Lett. **34** (1975) 706.

[41] J. S. Kang and H. J. Schnitzer, *"Dynamics of Light and Heavy bound Quarks"*, Phys. Rev. D **12** (1975) 841.

[42] J. S. Kang and Howard. J. Schnitzer, *"Is $\psi'(3700)$ a radial excitation of $\psi(3100)$?"*, Phys. Rev. D **12** (1975) 2791.

[43] B. J. Bjorlen and S. L. Glashow, *"Elementary Particles and SU(4)"*, Phys. Lett. 11, 255 (1964).

[44] S. L. Glashow, J. iliopoulos and L. Maini, *"Weak Interactions with Lepton-Hadron Symmetry"*, Phys. Rev. D 2, 1285(1970).

[45] Yasuo Hara, *"Unitary Triplets and the Eightfold Way"*, Phys. Rev. 134, B701 (1964).

[46] M. K. Gaillard and B. W. Lee, *"Rare Decay Modes of K Mesons in Gauge Theories"*, Phy. Rev. D 10, 897(1974).

[47] G. Goldhaber et al., *"Observation in e^+e^- Annihilation of a Narrow State at 1865 MeV/c2 Decaying to $K\pi$ and $K\pi\pi\pi$"*, Phys. Rev. Lett. 37, 255 (1976).

[48] B. R. Martin, *"Nuclear and Particle Physics"*, John Wiley & Sons Ltd, (2006).

[49] S. Okubo, *"ϕ-meson and unitary symmetry model"*, Phys. Lett. 5, 165 (1963).

[50] G. Zweig, *"An SU(3) Model for Strong Interaction Symmetry and its Breaking"*, CERN preprint 8419/TH.412; 8182/TH.401.(1964)

[51] Jugoro Iizuka, *"A Systematics and Phenomenology of Meson Family"*, Prog. Theor. Phys. Supplement No.37 & 38, 21-34 (1966).

[52] Stephen Godfrey and Jim Napolitano, *"Light Meson Spectroscopy"*, Rev. Mod. Phy. 71, 1411 (1999).

[53] O. M. Boyarkin, *"Introduction to Physics of Elementary Particles"*, Nova Science Publishers, Inc. New York (2007).

[54] B. R. Martin, G. Shaw, *"Particle Physics"*, Third Edition, John Wiley and Sons, 2008.

[55] Stephen Godfrey and Nathan Isgur, *"Mesons in a relativized quark model with chromodynamics"*, Phys. Rev. D 32, 189(1985).

[56] W. Braunschweig et al., *"Observation of the two photon cascade* $3.7 \rightarrow 3.1 + \gamma\gamma$ *via an intermediate state* P_c*"*, Phys.

[57] P. A. Rapidis et al., *"Observation of Resonance in* e^+e^- *Annihilation Just above Charm Threshold"*, Phy. Rev. Lett 39, 526(1977),

[58] J. S. Whitaker et al., *"Radiative Decays of $\psi(3095)$ and $\psi(3684)$"*, Phys. Rev. Lett. 37, 1596(1976).

[59] W. Tanenbaum et al., *"Radiative Decays of $\psi(3684)$ into High Mass States"*, Phys. RevD. 17, 1731 (1978).

[60] M.B. Voloshin, *"Charmonium"*, Prog. Part. Nucl. Phys. 61: 455-511, 2008.

[61] V.A. Novikov et al., *"Charmonium and Gluons"*, Physics Reports 41, 1-133, 1978.

[62] S. Bianco et al., *"A Cicerone for the Physics of Charm"*, arXive:0309021v1[hep-ex], 2003.

[63] Diego Bettoni and Roberto Calabrese, *"Review Charmonium Spectroscopy"*, Prog. Part. Nucl. Phys. 54: 615-651, 2005.

[64] L. Kpke, N. Wermes, *"J/ψ Decays"*, Physics Reports 174, 67-227 (1989). and CERN-EP-88-93 (1988)

[65] B. Richter, "From psi to charm: The experiments from 1975 and 1976", Rev. Mod. Phy. 49 251(1977).

[66] Frederick A. Harris, *"BEPCII and BESIII"*, Nuclear Physics B (Proc. Suppl.) 162 (2006) 345350.

[67] Kuang-Ta Chao and Yifang Wang, *"Physics at BESIII", IHEP-Physics-Report-BES-III-2008-001-v1*,arXiv:0809.1869v1.

[68] M. Ablikim et.al., *"Design and construction of the BESIII detector"*, Nuclear Instruments and Methods in Physics Research **A 614** (2010) 345-399.

[69] J.B. Liu et.al., *"A beam test of a prototype of the BESIII drift chamber in magnetic field"*, Nuclear Instruments and Methods in Physics Research **A 557** (2006) 436-444.

[70] Xihui Chen et.al., *"Design and implementation of the BESIII detector-control system"*, Nuclear Instruments and Methods in Physics Research **A 592** (2008) 428- 433.

[71] Miao He, *"Simulation and reconstruction of the BESIII EMC"*, Journal of Physics: Conference Series 293 (2011) 012025.

[72] M. Ablikim et al., *"Determination of the number of ψ' events at BESIII"* Chinese Physics C (HEP and NP), 33(X),(2009).

[73] J. Allison et al., *"Geant4 Developments and Applications"*IEEE Trans. Nucl. Sci. textbf53 (2006) 270.

[74] S.Agostinelli et al. *"GEANT4- a simulation toolkit"*,Nuclear Instruments and Methods in Physics Research **A 506** (2003) 250-303.

[75] W. D. Li, H. M. Liu et al. *"The offline Software for the BES-III Experiment"*, The Proceedings of the 15th International Conference on Computing in High Energy and Nuclear Physics (CHEP06) (Mumbai, India, 13-17 February 2006).

[76] G. Barrand et al., *"GAUDI A software architecture and framework for building HEP data processing applications"* Comput. Phys. Commun. **140** (2001) 45-55. .

[77] R. A. Briere et al., *"Observation of Thirteen New Exclusive Multibody Hadronic Decays of the $\psi(2S)$"*, Phys. Rev. Lett. **95** 062001(2005).